AMERICAN SOCIETY FOR MICROBIOLOGY | mBio

Genomics and Proteomics | Research Article

Uncovering the temporal dynamics and regulatory networks of thermal stress response in a hyperthermophile using transcriptomics and proteomics

Felix Grünberger,[1] Georg Schmid,[1] Zubeir El Ahmad,[1] Martin Fenk,[1] Katharina Vogl,[1] Robert Reichelt,[1] Winfried Hausner,[1] Henning Urlaub,[2,3] Christof Lenz,[2,3] Dina Grohmann[1]

AUTHOR AFFILIATIONS See affiliation list on p. 25.

ABSTRACT Facing rapid fluctuations in their natural environment, extremophiles, like the hyperthermophilic archaeon *Pyrococcus furiosus*, exhibit remarkable adaptability to extreme conditions. However, our understanding of their dynamic cellular responses remains limited. This study integrates RNA-sequencing and mass spectrometry data, thereby elucidating transcriptomic and proteomic responses to heat and cold shock stress in *P. furiosus*. Our results reveal rapid and dynamic changes in gene and protein expression following these stress responses. Heat shock triggers extensive transcriptome reprogramming, orchestrated by the transcriptional regulator Phr, targeting a broader gene repertoire than previously demonstrated. For heat shock signature genes, RNA levels swiftly return to baseline upon recovery, while protein levels remain persistently upregulated, reflecting a rapid but sustained response. Intriguingly, cold shock at 4°C elicits distinct short- and long-term responses at both RNA and protein levels. Cluster analysis identified gene sets with either congruent or contrasting trends in RNA and protein changes, representing well-separated arCOG groups tailored to their individual cellular responses. Particularly, upregulation of ribosomal proteins and significant enrichment of 5′-leadered sequences in cold-shock responsive genes suggest that translation regulation is important during cold shock adaption. Further investigating transcriptomic features, we reveal that thermal stress genes are equipped with basal sequence elements, such as strong promoter and poly(U)-terminators, facilitating a regulated response of the respective transcription units. Our study provides a comprehensive overview of the cellular response to temperature stress, advancing our understanding of stress response mechanisms in hyperthermophilic archaea and providing valuable insights into the molecular adaptations that facilitate life in extreme environments.

IMPORTANCE Extreme environments provide unique challenges for life, and the study of extremophiles can shed light on the mechanisms of adaptation to such conditions. *Pyrococcus furiosus*, a hyperthermophilic archaeon, is a model organism for studying thermal stress response mechanisms. In this study, we used an integrated analysis of RNA-sequencing and mass spectrometry data to investigate the transcriptomic and proteomic responses of *P. furiosus* to heat and cold shock stress and recovery. Our results reveal the rapid and dynamic changes in gene and protein expression patterns associated with these stress responses, as well as the coordinated regulation of different gene sets in response to different stressors. These findings provide valuable insights into the molecular adaptations that facilitate life in extreme environments and advance our understanding of stress response mechanisms in hyperthermophilic archaea.

KEYWORDS archaea, heat shock, cold shock, transcriptomics, proteomics

Invited Editor Xiuzhu Dong, Institute of Microbiology, Chinese Academy of Sciences, Beijing, China

Editor Joerg Vogel, University of Würzburg, Würzburg, Germany

Address correspondence to Felix Grünberger, felix.gruenberger@ur.de, or Dina Grohmann, dina.grohmann@ur.de.

The authors declare no competing interests. D.G. and G.S. are co-founders of Microbify GmbH. However, this study was not funded by Microbify GmbH.

See the funding table on p. 25.

Received 24 August 2023
Accepted 30 August 2023
Published 16 October 2023

The ability of extremophilic microorganisms to adapt and thrive in extreme environments has captivated the scientific community for decades (1–3). These organisms provide unique opportunities to investigate the molecular basis of stress response, adaptation, and recovery of cellular activities, offering valuable insights into fundamental biological processes and enabling novel biotechnological applications (4). Among extremophiles, the hyperthermophilic archaeon *Pyrococcus furiosus* has become a model organism for studying the molecular strategies employed by thermophiles to withstand high temperatures (5–7). *Pyrococcus* species are marine-living anaerobic organisms that grow over a broad temperature range from 70°C to 104°C and can be found in marine sediments and in black smokers within hydrothermal vent systems that are characterized by significant temperature gradients ranging from 2°C to 400°C (Fig. S1A at https://doi.org/10.6084/m9.figshare.24006960.v1) (8–11). Since hydrothermal vents are sterile during their initial formation, it was first hypothesized and later experimentally shown that they are colonized by hyperthermophilic archaea from the surrounding 4°C-cold seawater (12, 13). Moreover, evidence suggests that *Pyrococcus* must possess mechanisms to withstand extended cold-shock periods as it has been successfully recultivated from cooled-down submarine plumes and floating volcanic slick taken over 1 km away from the active zone of an erupted submarine volcano (14). This observation has also been replicated in the laboratory, where it was demonstrated that hyperthermophiles could survive for at least 9 months in cold environments and react within seconds upon returning to their optimal growth temperature by initiating motility (15).

In general, hyperthermophilic archaea have adapted to thrive at temperatures exceeding 80°C through various molecular mechanisms, including stabilization of tRNAs and rRNA by higher GC-content, enrichment in hydrophobic and charged amino acids, alterations in protein structure, unique membrane composition, increased investment in nucleoid-associated proteins, and positive DNA supercoiling by reverse gyrase (16–20). However, the biomolecular and biophysical challenges associated with heat shock above the individual temperature limit of each organism are at least, to some extent, shared across the domains of life (21, 22). In contrast, less is known about shared molecular principles dealing with cold shock response, especially in archaea (23, 24).

Extreme temperature fluctuations pose significant challenges to cellular macromolecules, such as proteins, nucleic acids, and lipids. For instance, elevated temperatures can lead to protein denaturation, aggregation, and loss of function during heat shock. Concurrently, DNA and RNA can undergo structural alterations, impairing replication, transcription, and translation processes (25). On the other hand, cold shock induces the stabilization of secondary structures in nucleic acids, impeding their proper function and reducing transcription and translation efficiency. Furthermore, low temperatures affect membrane fluidity, potentially impairing membrane-associated processes and transport (23, 24, 26).

In bacteria, the heat shock response is primarily regulated by the conserved sigma factor σ32, which promotes transcription of heat shock genes encoding chaperones, such as DnaK and GroEL, and proteases responsible for protein refolding and degradation (27). In addition to the positive regulation by sigma factors, it is well-known that transcriptional repressors, like HrcA or HspR, can also induce expression of heat shock genes by dissociating from the promoter (28–30). Cold shock responses involve the synthesis of cold-induced proteins, such as CspA in *Escherichia coli*, which counteract the effects of low temperatures on nucleic acids and cellular processes. These Csps are small, nucleic acid-binding proteins that are widely distributed in bacteria and structurally highly conserved, containing a cold shock domain that enables binding to target RNA and DNA. Also, they function as RNA chaperones, destabilizing secondary structures at low temperatures and facilitating transcription and translation (24, 31, 32).

In eukaryotes, the heat shock response is orchestrated by heat shock transcription factors, which modulate the expression of heat shock proteins like Hsp70 and Hsp90. On the other hand, the cold shock response involves diverse mechanisms, such as changes

in membrane lipid composition and synthesis of cold-inducible RNA-binding proteins (33–36).

Organisms across the tree of life are challenged by stressors such as heat and cold shock. The specific molecular players and regulatory networks involved in these processes, however, can differ significantly. For example, cold shock domain proteins are absent in all thermophilic and hyperthermophilic archaea, and the regulation of the cold shocks response in archaea is less well understood compared to bacteria and eukaryotes (37). However, for the heat shock response, some regulatory mechanisms have been identified, such as the transcription factor (TF) Phr in *P. furiosus*, which recognizes a palindromic DNA sequence and acts as a negative regulator of many heat-inducible genes (38–40). In contrast, no thermal-responsive regulator has been identified in Crenarchaeota and, thus, is also not present in the well-described thermophile *Sulfolobus acidocaldarius* (21, 41). Nevertheless, *S. acidocaldarius* exhibits a classic heat shock response characterized by the induction of small chaperones and the thermosome. Notably, its genome encodes two to three different thermosome subunits, and their assembly is modulated based on the prevailing environmental conditions (21, 42).

In addition to transcription factor-based regulation, archaeal-specific small RNAs (asRNAs) and RNA-binding proteins like proteins of the Sm-like protein family have been implicated in fine-tuning regulation of stress responses on the post-transcriptional level (43–46).

Despite significant advancements in the field, our understanding of the complex regulatory networks and adaptive mechanisms employed by *P. furiosus* in response to extreme temperature variations remains limited, especially when considering the time-related aspects of these processes on the RNA and protein level.

This study aims to unravel the temporal dynamics of thermal stress response in the hyperthermophilic archaeon *P. furiosus* using an integrative omics approach that combines transcriptomic and proteomic analyses at multiple time points. Our objective is to analyze shifts in gene expression and protein abundance that occur as the organism experiences conditions mimicking the thermal environment of hydrothermal vents. To achieve this, we first compare our findings with the established knowledge of responses on the transcriptional level and mechanisms of the heat and cold shock response. We, furthermore, integrate the transcriptomic and proteomic data to generate a more comprehensive understanding. Moreover, we consider the temporal resolution of our experimental setup to identify gene clusters and key cellular processes that display similar regulatory patterns. Furthermore, we explore putative regulatory elements, such as promoters, terminators, and operons, that may influence the transcriptomic landscape under stress conditions. In particular, we seek to enhance our understanding of the temporal resolution of Phr-regulated heat shock response. Ultimately, this in-depth analysis aims to expand our knowledge of the molecular adaptations that enable long-term survival in cold seawater and recolonization of black smokers, contributing to the broader understanding of extremophile biology.

MATERIALS AND METHODS

Growth conditions and sample preparations

Pyrococcus furiosus DSM 3638 was cultured in 120 mL serum bottles following the protocol previously described under anaerobic conditions at one bar excess of nitrogen (47). Cells were grown in 40 mL SME medium supplemented with 40 mM pyruvate, 0.1% peptone, and 0.1% yeast extract for 15 h at 95°C until they reached the mid-exponential growth phase with a cell density of 5×10^7 cells/mL (47).

For cold shock treatment, cells in the mid-exponential growth phase were subjected to cold shock by rapidly cooling the medium through a 2.5-m long, 2-mm diameter viton hose flushed with anaerobic NaCl solution into a new bottle containing 1 bar excess of nitrogen (Fig. S1B and C at https://doi.org/10.6084/m9.figshare.24006960.v1). The transfer took 90 s, and the time to reach 4°C in an ice water bath was 160 s in total,

which marked the beginning of the cold shock treatment. For recovery, the ice bath was replaced with a 95°C hot water bath, and a recovery sample was collected 5 min after the target temperature of 95°C was reached.

For heat shock treatment, serum bottles with cells in the mid-exponential growth phase were placed in a 105°C incubator. It took 26 min for the cultures to reach the target temperature of 105°C, which was considered the starting point for the heat shock treatment. Samples were collected after 5 and 15 min of incubation at this temperature. For recovery, cultures were transferred to another incubator and allowed to cool down to 95°C, which took 10.5 min (Fig. S1D at https://doi.org/10.6084/m9.figshare.24006960.v1).

Cells from all conditions were harvested by centrifugation at 14,000 × *g* for 10 min at 4°C and resuspended in 2 mL buffer (25 mM Tris/HCl pH 7.6, 100 mM NaCl). Samples were then divided for RNA (1.5 mL) and protein analysis (0.5 mL), followed by centrifugation at 17,700 × *g* for 5 min at 4°C. The resulting pellets were stored at −80°C until further analysis.

RNA extraction

Total RNA isolation was performed using cell pellets, which were initially lysed by adding 1 mL of TRI Reagent (Zymo Research) and subsequently processed with the Direct-zol RNA Miniprep Plus kit (Zymo Research) following the manufacturer's instructions. This protocol included DNase I digestion to eliminate genomic DNA contamination.

To evaluate the purity, quality, and quantity of the extracted RNA, several analytical methods were employed. Standard spectroscopic measurements were performed using a NanoDrop One spectrophotometer (Thermo Fisher Scientific). Fluorometric quantification was carried out with the Qubit RNA assay (Thermo Fisher Scientific). Lastly, RNA integrity values were assessed using a Bioanalyzer (Agilent Technologies) to ensure the suitability of the RNA samples for downstream applications.

RNA sequencing for differential gene expression analysis

Library preparation and sequencing

Four independent biological replicates were prepared for each condition and subjected to differential gene expression analysis. Prior to library preparation, ribosomal RNAs were depleted from 1 µg input RNA using the Pan-Archaea riboPOOL (siTOOLs) according to the manufacturer's instructions. Library preparation and RNA-seq were carried out as described in the Illumina "Stranded mRNA Prep Ligation" Reference Guide, the Illumina NextSeq 2000 Sequencing System Guide (Illumina, Inc., San Diego, CA, USA), and the KAPA Library Quantification Kit—Illumina/ABI Prism (Roche Sequencing Solutions, Inc., Pleasanton, CA, USA). In brief, omitting the initial mRNA purification step with oligo(dT) magnetic beads, around 5 ng of rRNA-depleted archaeal RNA was fragmented to an average insert size of 200–400 bases using divalent cations under elevated temperature (94°C for 8 min). Next, the cleaved RNA fragments were reverse transcribed into first-strand complementary DNA (cDNA) using reverse transcriptase and random hexamer primers. Actinomycin D was added to allow RNA-dependent synthesis and to improve strand specificity by preventing spurious DNA-dependent synthesis. Blunt-ended second strand cDNA was synthesized using DNA Polymerase I, RNase H, and dUTP nucleotides. The incorporation of dUTP, in place of dTTP, quenches the second strand during the later PCR amplification because the polymerase does not incorporate past this nucleotide. The resulting cDNA fragments were adenylated at the 3′ ends, and the pre-index anchors were ligated. Finally, DNA libraries were created using a 15 cycle PCR to selectively amplify the anchor-ligated DNA fragments and to add the unique dual indexing (i7 and i5) adapters. The libraries were bead purified twice and quantified using the KAPA Library Quantification Kit. Equimolar amounts of each library were sequenced on an Illumina NextSeq 2000 instrument controlled by the NextSeq 2000 Control Software (NCS, v. 1.4.1.39716), using one 50 cycles P3 Flow Cell with the dual index, single-read (SR) run parameters. Image analysis and base calling were done by

the Real-Time Analysis Software (RTA) (v. 3.9.25). The resulting .cbcl files were converted into .fastq files with the bcl2fastq software (v. 2.20).

Library preparation and sequencing were performed at the Genomics Core Facility "KFB - Center of Excellence for Fluorescent Bioanalytics" (University of Regensburg, Regensburg, Germany; www.kfb-regensburg.de).

Differential gene expression analysis

Raw sequencing reads in fastq format were filtered for quality and trimmed using fastp (v. 0.23.2) to remove low-quality bases and adapter sequences (--cut_front --cut_tail -q 30) (48). Reads mapping to ribosomal RNAs were bioinformatically removed from the trimmed reads using the sortmeRNA tool (v. 4.3.6) based on sequences in the SILVA database. In the next step, the rRNA-depleted reads were aligned to the *Pyrococcus furiosus* DSM 3638 reference genome (NCBI: CP023154.1) using Bowtie2 (v. 2.5.0) with default parameters (49). The resulting sequence alignment files (SAM) were converted to binary mapping format (BAM) using samtools (v. 1.17) (50).

Differentially expressed genes from RNA-seq count data were identified following the recommendations in the Bioconductor vignette of the DESeq2 package (v. 1.36) (51). Briefly, featureCounts (RSubread package v. 2.10.5) was used to calculate the count matrix based on a custom GTF file generated by filtering the *P. furiosus* DSM 3638 GFF annotation file downloaded from the NCBI for protein-coding genes (column biotype) (52). Principal component analysis (PCA) was performed on variance stabilizing transformed data, and outlier replicates (HS 1 replicate 1, HS 2 replicate 4, HS R replicate 1, CS R replicate 2) were removed from the data set after visual inspection. Differential expression analysis was conducted by comparing each of the cold or heat shock conditions with the control condition in a pairwise manner.

Term-seq

Library preparation and sequencing

For efficient 3′ adapter ligation, 1 µg DNase-treated RNA (control condition, 95°C, mid-exponential growth phase) was mixed with 1 µL RNA 3′ adapter containing four degenerate bases (5′-amino-NNNNAGATCGGAAGAGCGTCGTGTAGGGAAAG-phosphate-3′, Microsynth, 150 µM), 2.5 µL 10× T4 RNA ligase buffer, 2.5 µL ATP (10 mM), 2 µM DMSO (100%), 9 µL PEG8000 (50%), 2.5 µL T4 RNA ligase 1 (10 U/µL, NEB), and 0.5 µL RiboLock RNase Inhibitor (40 U/µL) and filled up to a total volume of 25 µL. The reaction was incubated at 23°C shaking (450 rpm) for 2.5 h and cleaned up with 2.2 × vol AMPure XP Beads.

Subsequently, rRNAs were depleted using the Pan-Archaea riboPOOL (siTOOLs) according to the manufacturer's instructions. 3′-Ligated and rRNA-depleted RNAs were split in half and fragmented by adding 1 µL 10× RNA Fragmentation Reagent (Ambion) and incubation at 70°C for 7.5 min and 15 min, respectively. The reactions were stopped by the addition of 1 µL stopping solution (200 mM EDTA pH 8.0) and pooled and cleaned up with 2.2× vol AMPure XP Beads. For cDNA synthesis, fragmented RNAs were first mixed with 1 µL RTP primer (5′- TCTACACTCTTTCCCTACACGACGCTCTTC-3′, 10 µM) and incubated for 5 min at 65°C. Subsequently, samples were placed on ice and 4 µL 5× First-Strand Buffer, 1 µL DTT (100 mM), 2 µL dNTPs (10 mM), and 2 µL SuperScript III (200 U/µL) was added. Synthesis was performed for 60 min at 50°C after which the enzyme was heat inactivated for 15 min at 70°C. Next, RNase digestion was performed by adding 1 µL RNaseH (5 U/µL) and incubating the samples for 30 min at 37°C. The reaction was cleaned using 2.2 × vol AMPure XP beads. To reduce primer dimer formation, cDNA was mixed with 1 µL 10 µM 3′ RNA adapter and denatured for 3 min at 95°C in a thermoblock. Subsequently, the samples were cooled to 23°C with an initial cooling rate of 10 s/°C until 72°C was reached at which the cooling rate was lowered to 15 s/°C. Next, 2.5 µL 10× T4 RNA ligase buffer, 2.5 µL ATP (10 mM), 2 µM DMSO (100%), 9.5 µL PEG8000 (50%), 2.5 µL T4 RNA ligase 1 (10 U/µL, NEB), and 1 µL

3′ cDNA adapter (5′-amino- NNNNAGATCGGAAGAGCACACGTCTGAACTCCAGTCAC-phosphate-3′, Microsynth, 150 µM) were added to the hybridized cDNA, incubated at 23°C shaking (450 rpm) for 6 h and cleaned up with 2.2× vol AMPure XP beads. Finally, cDNA libraries were amplified using a 12 cycle PCR with NEBNext Multiplex Oligos for Illumina protocol (NEB) and a standard Phusion polymerase protocol (NEB). Amplified libraries were cleaned up after gel electrophoresis (selected size between 200 and 500 bp) by a NucleoSpin Gel and PCR Clean-up kit (Macherey-Nagel) according to the manufacturer's instructions for high-percentage agarose gels.

Sequencing was performed at the Genomics Core Facility "KFB - Center of Excellence for Fluorescent Bioanalytics" (University of Regensburg, Regensburg, Germany; www.kfb-regensburg.de) and carried out as described in the Illumina NextSeq 500 System Guide (Illumina, Inc., San Diego, CA, USA), and the KAPA Library Quantification Kit—Illumina/ABI Prism (Roche Sequencing Solutions, Inc., Pleasanton, CA, USA). In brief, the libraries were quantified using the KAPA Library Quantification Kit. Equimolar amounts of each library were sequenced on a NextSeq 500 instrument controlled by the NextSeq Control Software (NCS, v. 2.2.0), using one 75 Cycles High Output Kits with the single index, paired-end (PE) run parameters. Image analysis and base calling were done by the Real-Time Analysis Software (RTA, v. 2.4.11). The resulting .bcl files were demultiplexed and converted into .fastq files with the bcl2fastq software (v. 2.18).

The Term-seq protocol was applied to four biological replicates of cells grown to mid-exponential growth phase at 95°C.

Identification of enriched 3' ends

Fastq files were quality and adapter trimmed using trimmomatic (v. 0.39) in paired-end mode (ILLUMINACLIP:TruSeq3-PE.fa:2:30:10:8:true, AVGQUAL:25, MINLEN:20) (53). Unique molecular identifiers (UMIs) were extracted from paired-end reads by UMI-tools (v. 1.0.1) using the umi_tools command (--bcpattern=NNNN, --bc-pattern2=NNNN). Mapping was performed by bowtie2 (v. 2.2.5) in --sensitive-local mode with the last four nucleotides of each read being trimmed using --trim3 4 (54). SAM files were converted to BAMs and sorted and indexed using samtools (v. 1.9) (50). Subsequently, mapped reads were deduplicated using the extracted UMIs by umi_tools dedup (v. 1.0.1) with default settings for paired-end data. Detection of enriched 3′ ends by peak calling and downstream analysis was performed as described in reference (55). Briefly, strand-specific bedgraph files were first generated and CPM (counts per million normalization for sequencing depth) normalized using deepTools bamCoverage (v. 3.5.0), with the SAM flags 83 and 99 in combination with --Offset 1 and --binSize 1 --minMappingQuality 20. Next, the termseq_peaks script was used with default parameters to call peaks using four replicates as input (https://github.com/nichd-bspc/termseq-peaks) (56). For end detection, peak files were merged with the position-specific count files using bedtools intersect (option -wao, v. 2.31.0). Enriched positions were finally filtered and annotated based on the following criteria: For each peak, the position with the highest number of reads was selected per replicate and only maximum peak positions selected that were present in at least three of the four replicates. Positions with less than five CPM counts were excluded from the analysis. Positions were assigned based on their relative orientation to a gene and their respective peak height as primary (highest peak within 300 bases downstream from a gene), secondary (each additional peak 300 bases downstream from a gene), and internal (each peak in the coding range).

Nanopore sequencing

Library preparation and sequencing

For PCR-cDNA sequencing, ribosomal RNAs were first depleted using the Pan-Archaea riboPOOL (siTOOLs) according to the manucfacturer's instructions with 1 µg DNase-treated input RNA (control condition, 95°C, mid-exponential growth phase). To prevent secondary structure formation and inefficient RNA treatment, samples were

heat-incubated at 70°C for 3 min and immediately placed on ice before ligation. Next, a custom 3′ adapter (5′-rAppCTGTAGGCACCATCAAT–NH2-3′, NEB) was ligated to all RNAs following the protocol described in reference (57). This protocol is an alternative to the otherwise necessary enzymatic polyadenylation and improves 3′ end accuracy (58). Briefly, 100 ng rRNA-depleted RNA was mixed with 50 pmol 3′ adapter, 2 µL 10 × T4 RNA ligase reaction buffer (NEB), 10 µL 50% PEG 8000 (NEB), 1 µL 40 U/µL-1 RNase Inhibitor (NEB), and 1 µL T4 RNA ligase 2 (truncated K227Q, NEB, 200,000 units/mL) and incubated at 16°C for 14 h. Finally, RNAs were cleaned up using the ZYMO RNA Clean and Concentrator kit (ZYMO).

PCR-cDNA sequencing libraries were prepared following the Oxford Nanopore Technologies (ONT) PCR-cDNA barcoding kit protocol (SQK-PCB109) with minor modifications, such as using a custom 3′ cDNA RT primer (5′-ACTTGCCTGTCGCTCTATCTT-CATTGATGGTGCCTACAG-3′, 2 µM), which replaces the VN primer. RNA and cDNA sizes were assessed using a Bioanalyzer (Agilent). After reverse transcription and template-switching as described in the ONT protocol, samples were PCR-amplified for 12 cycles with a 500-s elongation time. During library preparation, samples were quantified and quality checked using standard spectroscopic measurements (Nanodrop One, Thermo Fisher Scientific) and Qubit assays (Thermo Fisher Scientific). Equimolar amounts of samples were pooled, adapter-ligated, and sequenced on an R9.4 flow cell (Oxford Nanopore Technologies) using an MK1C device for 72 h.

PCR-cDNA sequencing was performed for two biological replicates of cells grown to mid-exponential growth phase at 95°C.

Data analysis of PCR-cDNA libraries

Basecalling of fast5 files was performed using guppy (v. 6.4.2+97a7f06) in high-accuracy mode (dna_r9.4.1_450bpd_hac.cfg) with standard parameters and a quality score threshold of 9. The PCR-cDNA library was demultiplexed by guppy_barcoder using default settings (–barcode_kits SQK-PCB109), except for disabling barcode trimming. Full-length sequenced reads were identified, strand-oriented, and trimmed using pychopper (v. 2.7.2, https://github.com/epi2me-labs/pychopper) with autotuned cutoffs and the recommended edlib backend for identifying custom primers. Cutadapt (v. 4.2) was used to remove remaining 3′-adapter sequences with the parameters -a "CTGTAG-GCACCATCAAT" -j 0. Next, trimmed reads were mapped using minimap2 (v. 2.24-r1122) with standard parameters suggested for aligning Nanopore genomic reads (-ax map-ont) to the *P. furiosus* DSM 3638 genome (NCBI: CP023154.1) (59, 60). Alignments with more than five clipped bases (soft or hard clips) were removed using samclip (v. 0.4.0), and SAM files were converted to sorted BAM files using samtools (v. 1.16.1) (50).

Lastly, strand-specific coverage files were created using samtools depth (-a, -J options enabled) with a binsize of 1 and including reads with deletions in the coverage computation. Downstream analysis, including CPM normalization, calculating the mean coverage for each position of the two replicates, and plotting, was performed using the Tidyverse (v. 2.0.0) in R (61).

Mass spectrometry

Sample preparation, analysis, and data processing

Mass spectrometry analysis was performed for four biological replicates according to the following protocol. Protein samples were first purified by running them a short distance into a 4%–12% NuPAGE Novex Bis-Tris Minigel (Invitrogen), followed by Coomassie staining and in-gel digestion with trypsin (62).

For generation of a peptide library, equal amount aliquots from each sample were pooled to a total amount of 200 µg and separated into 12 fractions using a basic pH reversed phase C18 separation on an FPLC system (Äkta pure, Cytiva) and a staggered pooling scheme. All samples were spiked with a synthetic peptide standard used for retention time alignment (iRT Standard, Schlieren, Schweiz).

Protein digests were analyzed on a nanoflow chromatography system (nanoElute) hyphenated to a hybrid timed ion mobility-quadrupole-time-of-flight mass spectrometer (timsTOF Pro, all Bruker). In brief, 400 ng equivalents of peptides were dissolved in loading buffer (2% acetonitrile, 0.1% trifluoroacetic acid in water), enriched on a reversed-phase C18 trapping column (0.3 cm × 300 µm, Thermo Fisher Scientific) and separated on a reversed-phase C18 column with an integrated CaptiveSpray Emitter (Aurora 25 cm × 75 µm, IonOpticks) using a 60 min linear gradient of 5%–35% acetonitrile/0.1% formic acid (vol:vol) at 300 nL min^{-1}, and a column temperature of 50°C.

DDA analysis was performed in PASEF mode (63) with 10 PASEF scans per topN acquisition cycle. Multiply charged precursors were selected based on their position in the *m/z*-ion mobility plane and isolated at a resolution of 2 Th for $m/z \leq 700$ and to 3 Th for $m/z > 700$ for MS/MS to a target value of 20,000 arbitrary units. Dynamic exclusion was set to 4 min. Two technical replicates per C18 fraction were acquired.

DIA analysis was performed in diaPASEF mode (64) using 32 × 25 Th isolation windows from *m/z* 400 to 1,200 to include the 2+/3+/4+ population in the *m/z*-ion mobility plane. The collision energy was ramped linearly as a function of the mobility from 59 eV at 1 /K0 = 1.6 Vs cm^{-2} to 20 eV at 1 /K0 = 0.6 Vs cm^{-2}. Two technical replicates per biological replicate were acquired.

Protein identification and quantification were performed in Spectronaut Software 15.6 (Biognosys). Protein identification was achieved using the software's Pulsar algorithm at default settings against the UniProtKB *Pyrococcus furiosus* reference proteome (revision 09-2021) augmented with a set of 51 known common laboratory contaminants. For quantitation, up to the 6 most abundant fragment ion traces per peptide and up to the 10 most abundant peptides per protein were integrated and summed up to provide protein area values. Mass and retention time calibration as well as the corresponding extraction tolerances was dynamically determined. Both identification and quantification results were trimmed to a False Discovery Rate of 1% using a forward-and-reverse decoy database strategy. Protein quantity distributions were normalized by quartile normalization, and intensity-based absolute quatification (iBAQ) values as proxies for protein levels (65).

Differential enrichment analysis

Quantitative values were processed using $\log_2$ transformation, and PCA was used for quality control and detection of outlier replicates (CS 2 replicate 1, CS 3 replicate 4, CS R replicate 2, HS 2 replicate 3, HS R replicate 1) after visual inspection. Normalized protein expression data were analyzed using the R limma package (v. 3.52.4) to identify differentially expressed proteins between control and cold or heat-stressed samples (66).

Additional bioinformatic analysis

Comparison of transcriptomic and proteomic data

For comparison of transcriptomic and proteomic results, either $\log_2$-fold changes or count values were compared. While iBAQ values were used as proxies for protein abundance, total transcripts per million (TPM) was used as a normalization method for RNA-seq data to account for differences in sequencing depth and transcript length. TPM values were calculated by dividing the number of reads mapping to each gene by the gene length in kilobases, then dividing the resulting reads per kilobase (RPK) values by the sum of all RPK values in the sample, and, finally, multiplying the quotient by one million. This normalization method ensures that the sum of all TPM values in each sample is the same, allowing for better comparison of gene expression levels between samples.

Additionally, TPM counts were used for visualization purposes throughout the manuscript for the transcriptomics data.

Functional enrichment analysis based on arCOG classification

To gain insights into functional characteristics of differentially expressed genes, functional enrichment analysis based on the Archaeal Clusters of Orthologous Genes (arCOG) classification was performed as described previously (67, 68). Briefly, arCOGs for *P. furiosus* were retrieved from (69) and gene set enrichment analysis performed with the goseq package (v. 1.48.0) in R, which accounts for gene lengths bias (70). For each comparison, a condition- and method-specific background file was generated from all genes that could be detected. Next, *P*-values for overrepresentation of arCOG terms in the differentially expressed genes were calculated separately for up- and downregulated genes based on RNA-seq and MS data, respectively. Significant enrichments were identified with a threshold set at 0.05.

Promoter and terminator analysis

Primary transcription start sites (TSS) and corresponding 5′ UTR lengths were extracted from (47). Genes were categorized by the existence of an archaeal-typical promoter motif containing a TFB-recognition element [BRE, 5′-G/C(A/T)AAA-3′] and a TATA element [5′-TTT(A/T)(A/T)(A/T)−3′] (47, 71). Therefore, the sequences from −50 to +10 from the TSS were analyzed via MEME (v. 5.4.1., -mod zoops -minw 8 -maxw 20), resulting in a classification of genes contributing (+promoter) and not contributing (−promoter) to the motif (72). Position-specific motifs were plotted in R using the ggseqlogo package (v. 0.1) (73). Promoter strength was estimated according to the method used in reference (74). Briefly, sequences from −42 to −19 were extracted and analyzed using MEME in oops mode. The *P* value from the motif search was used as an estimator for the promoter strength. A lower *P*-value is indicative for a stronger promoter with a low propability of the archaeal promoter motif being found randomly.

3′ ends were classified similarly based on the presence of a poly(U)-terminator motif. To this end, sequences from −35 to +2 from the primary 3′ ends were extracted and analyzed via MEME (-mod zoops -minw 4 -maxw 20) and genes contributing to the motif classified as +poly(U) motif. Nucleotide enrichment analysis was performed as described in reference (75). Briefly, the frequency of each base was calculated using the extracted sequences and compared to the same calculation based on randomly sampling 100,000 positions from intergenic regions. Values from this comparison were $\log_2$ transformed and only the enrichment position of nucleotide U plotted.

Additionally, structural stability of the RNA was predicted by folding the 45 nt long RNA upstream of the terminators using the LncFinder package (v. 1.1.5) in R. This package utilizes the RNAfold software (v. 2.4.18) with standard parameters to predict the minimum free energy of the RNA structure. We compared these values to the calculated values from 1,000 randomly subsampled intergenic regions (76).

Operon analysis

Operon analysis of selected heat-shock genes was performed by comparing the annotation from the DOOR2 operon database, the operon annotation based on ANNOgesic prediction using short-reads from mixed conditions from *P. furiosus* and from single-read analysis of PCR-cDNA Nanopore reads generated for this study (47, 77). Selected genes were predicted to be a single gene unit or part of a multi-unit operon by visual inspection based on the gene overlap of single transcripts.

Correlation analysis

The Pearson correlation coefficient was employed as a general measurement of similarity between the count values or fold changes in a pairwise complete manner and was calculated using the ggpubr package (v. 0.6.0) in R.

For evaluating the similarity of the heat-shock and cold-shock results with a previously published heat-shock study, we compared the $\log_2$-fold changes from each

condition (relative to the control condition) with the expression changes extracted from Supplementary Tables S2 and S3 in reference (78). This allowed us to quantify the extent of similarity between the heat-shock, cold-shock, and recovery conditions and the temperature shift from 90°C to 97°C as described in reference (78).

Detection and analysis of signature clusters

The *z*-score normalized $\log_2$-fold changes of RNA and protein values were subjected to PCA using the prcomp function in R. Next, the PCA results were used to calculate the pairwise Euclidean distances between samples. This distance matrix serves as a measure of similarity between samples, enabling us to group genes that share similar profiles. To gain further insights into shared patterns, we performed hierarchical clustering with the ward.D2 linkage method.

The number of clusters was determined using the elbow method and after inspection of enrichment analysis of arCOG categories. This approach allowed for the identification of clusters of genes with similar expression patterns across different conditions and data sets, which could provide insights into the regulation of cellular processes in the hyperthermophilic archaeon *Pyrococcus furiosus*.

Functional analysis was performed using the STRING database to identify known and predicted protein-protein interactions among the differentially expressed genes (79).

The codon adaption index (CAI), a common index that measures how well the genes' codons are adapted to the organism's preferred codon usage, was imputed using the CAI function from the coRdon (v. 1.14.0) package using the 5% most abundant proteins according to our control sample (80).

RESULTS

Experimental setup and analysis strategy for studying the heat and cold shock response in *Pyrococcus furiosus*

To investigate the temporal dynamics of transcriptomic and proteomic responses of *P. furiosus* to heat and cold shock, we designed a custom temperature-controlled system for rapid cooling and reheating of samples (Fig. S1B at https://doi.org/10.6084/m9.figshare.24006960.v1). Cells were initially cultivated at an optimal temperature of 95°C to mid-exponential growth phase, serving as the control condition (Ctrl). Cold shock (CS) was simulated by shifting the temperature to 4°C, with samples taken at 20 min (CS 1), 2 h (CS 2), and 24 h after transfer of the samples to 4°C (CS 3) (Fig. 1A). This choice of 4°C as the cold shock temperature was carefully considered to replicate a biologically relevant yet standardized thermal stress condition, which simulates the extreme temperature fluctuations encountered by marine extremophiles, even for organisms isolated from geothermally heated sediments like *P. furiosus* that face unknown temperature gradients. Heat shock (HS) samples were collected after 5 min (HS 1) and 15 min (HS 2) after shifting the temperature to 105°C, a temperature that inhibits cell growth (8). In both setups, recovery samples (CS R, HS R) were obtained by returning cells to their optimal growth temperature following the final shock time point.

We performed deep RNA sequencing (RNA-seq) on rRNA-depleted libraries, yielding approximately 600-fold transcriptome coverage and detecting 95% (Ctrl), 91% (CS), and 92% (HS) of all 2,003 protein-coding transcripts in *P. furiosus* (Fig. 1B) (counts listed in Table S1 at https://doi.org/10.6084/m9.figshare.24007020.v1) (47). Additionally, we conducted mass spectrometry (MS) analysis on all samples, detecting 65% (Ctrl), 62% (CS), and 60% (HS) of the proteins, respectively. iBAQ values were used as accurate proxies for protein abundance. Nearly all proteins detected by MS with an IBAQ value of ≥10 had corresponding transcripts with at least 10 transcripts per million (TPM) RNA counts (Fig. 1B through D). Uniform distribution of TPM-normalized RNA-seq counts and iBAQ values suggests high data quality, allowing for comparisons between conditions and methods (Fig. 1C and D).

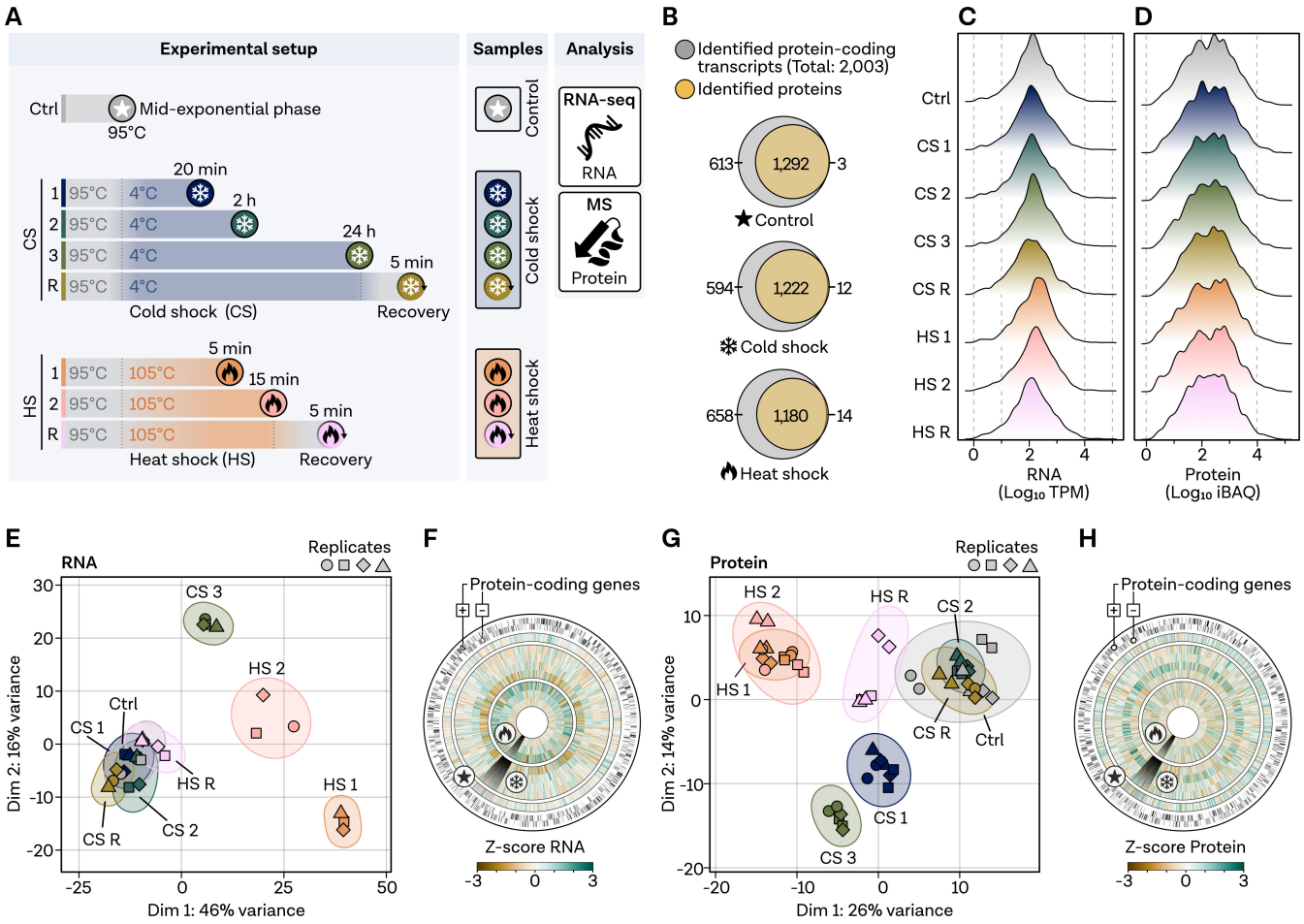

FIG 1 Validation of the experimental setup by temporal analysis of the heat and cold shock response in *Pyrococcus furiosus* via transcriptomics and proteomics. (A) Experimental design illustrating the seven stress-related conditions, including cold shock (CS) at 4°C and heat shock (HS) at 105°C, along with recovery samples, analyzed using RNA-seq and proteomics, compared to the control condition (Ctrl) at the optimal growth temperature of 95°C. (B) Venn diagram displaying the overlap between identified protein-coding transcripts (gray) and total identified proteins (yellow) under stress-related and control conditions. Genes only identified using RNA-seq or proteomics are shown at the left and right side, respectively. (C) Distribution of transcripts per million (TPM) normalized transcript counts, color-coded based on the legend in panel A. (D) Distribution of intensity-based absolute quantification (iBAQ) values for proteomics samples. (E) Principal component analysis of RNA-sequencing samples based on total counts; replicates are indicated using different symbols, with outliers removed. (F) Circular genome-wide plot of the *P. furiosus* genome (position 0 at top) with protein-coding genes on the two outer rings; *Z*-score normalized TPM counts color-coded by dark brown (negative) to dark green (positive) for each condition in the following order (outer to inner): Ctrl, CS 1, CS 2, CS 3, CS R, HS 1, HS 2, HS R. (G) PCA and (H) genome-wide circular plot for mass spectrometry samples analogous to panels E and F.

Principal component analysis (PCA) revealed distinct temporal and temperature-dependent responses at the RNA level, with the most significant variance observed after HS 1, HS 2, and CS 3 (Fig. 1E). To determine whether differences in the PCA can be explained by stress islands in the genome, we visualized z-score normalized TPM counts globally, finding that transcript changes were dispersed throughout the transcriptome (Fig. 1F). Variance at the RNA level was corroborated at the protein level, with two exceptions (Fig. 1G). First, the HS recovery sample did not cluster with the Ctrl condition but was positioned between HS 1 and the control, suggesting a prolonged protein response. Second, CS 1 formed a separate group at the protein level, reflecting substantial variation in protein expression patterns. Similar to the RNA level, proteome changes during CS and HS were not restricted to specific islands (Fig. 1H).

Transcriptome analysis reveals extensive reprogramming during heat shock and moderate overlapping response with the cold shock response in *P. furiosus*

Having verified the robustness of our experimental design for analyzing temporal aspects of thermal stress and recovery responses in *P. furiosus*, we proceeded with our investigation in two stages. Therefore, we first conducted a comprehensive transcriptome analysis to validate the selected time points and temperatures based on known stress responses and to identify potential regulatory aspects before integrating the results with the proteomics data. A 5-min HS at 105°C (HS 1) induced significant changes in 68% of the transcriptome, with 330 genes upregulated over 2-fold and 411 genes downregulated over 2-fold (Fig. 2A). Notably, several upregulated genes included well-known HS proteins, confirming the effectiveness of our experimental setup. Specifically, HS in *P. furiosus* has been shown to induce the expression of the thermosome (log_2FC: 2.7), small chaperones, such as HSP20 (log_2FC: 5.4), VAT1 (log_2FC: 6.7), and VAT2 (log_2FC: 0.2), and proteases that bind, refold, or degrade misfolded proteins accumulating in cells (7) (Fig. 2B). Moreover, we could confirm previous data showing that the synthase (Myo-inositol-1-phosphate synthase: Myo-Synthase, PF1616; log_2FC: 4.0) catalyzing a precursor of the compatible solute Di-myo-inositol-phosphate (DIP) accumulates during HS. DIP is suggested to have a protein-stabilizing role in hyperthermophiles, while proteins typically involved in controlling the thermal damage of the proteome, like the ATP-independent chaperone prefoldin (log_2FC: −1.1), are not upregulated during HS (78, 81). Some of the aforementioned proteins are under the control of the negative transcriptional regulator Phr. We confirmed that all currently known target genes, except PF1292, are substantially upregulated under our selected conditions (40). While the expression of the only ATP-dependent protease in *P. furiosus*, the proteasome (alpha-subunit log_2FC: −0.4; beta-subunit log_2FC: 0.2), is not increased during HS, the proteasome-assembling chaperone homolog PbaA (log_2FC: 3.9) that forms a complex with PF0014 (log_2FC: 3.9) is highly upregulated (7, 82) (Fig. 2B).

For systematic HS response analysis, we conducted functional enrichment analysis based on archaeal clusters of orthologous groups (arCOGs) (Fig. 2C) (69). Genes related to replication, recombination, and repair (category L) are overrepresented among highly upregulated genes. In contrast, genes associated with energy production (category C), motility (category N), cell defense (category V), inorganic ion transport (category P), amino acid transport (category E), and unknown groups are overrepresented among highly downregulated genes. The remaining significantly regulated genes with minor fold changes smaller than two do not exhibit clear categories, except for cell cycle (category D) overrepresentation in the upregulated group.

In comparison to HS, much less is known about the CS reaction in *Pyrococcus*. Our experimental setup significantly differs from previous analyses, which employed a temperature at which *Pyrococcus* can still grow (70°C), thus limiting direct comparisons (83). Upon immediate CS, 47% of the transcriptome underwent significant alterations (Fig. 2D). However, fewer protein-coding transcripts were strongly affected during CS 1 compared to HS 1, with only 78 strongly upregulated and 137 strongly downregulated genes observed. The most substantial upregulation occurred for a riboflavin-synthesis operon (PF0061–PF0064, log_2FC: 4.5), potentially under the control of the transcriptional regulator RbkR (PF0988) (84). Among the cold-responsive solute-binding proteins CipA (log_2FC: 1.5) and CipB (log_2FC: 0.2), only the former was induced significantly during CS (83). Functional enrichment analysis revealed that genes related to coenzyme transport and metabolism (category H) were overrepresented in highly upregulated genes during CS (Fig. 2E). Additionally, energy production (category C), carbohydrate transport (category G), and lipid transport (category I) were overrepresented in upregulated genes. In contrast, genes associated with amino acid transport and metabolism (category E) were downregulated on the RNA level during CS. Interestingly, genes involved in translation and ribosome function (category J), as well as inorganic ion transport (category P), remained unaffected at the RNA level. The functional overlap between

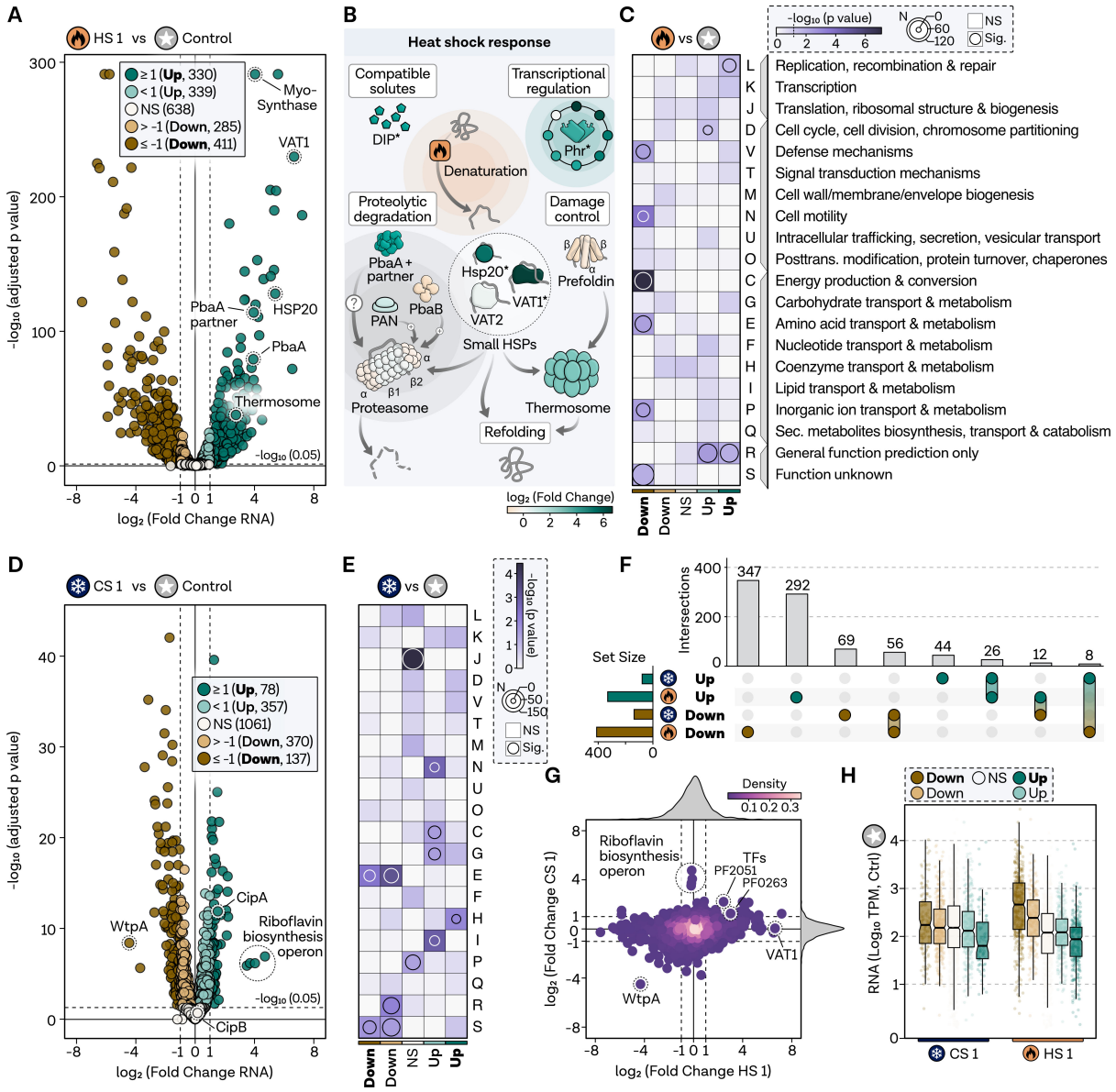

FIG 2 Immediate heat shock leads to extensive reprogramming on the transcriptome level with moderate overlap to cold shock response. (A) Volcano plot displaying $\log_2$-fold changes (*x*-axis) and significance ($-\log_{10}$ adjusted *P*-value, *y*-axis) comparing transcriptome changes at HS 1 (5 min) to the control condition. Protein-coding transcripts are categorized by significance and fold changes, color-coded as strongly upregulated (padj < 0.05 and $\log_2$FC ≥ 1, dark green, bold font), upregulated (padj < 0.05 and $\log_2$FC < 1 and $\log_2$FC > 0, light green, normal font), non-regulated genes (NS, padj ≥ 0.05, white), strongly downregulated (padj < 0.05 and $\log_2$FC ≤ −1, dark brown, bold font), downregulated (padj < 0.05 and $\log_2$FC > −1 and $\log_2$FC < 0, light brown, normal font). HS genes are highlighted. Significance level of 0.05 is shown as a dashed line. (B) Schematic representation of the HS response in *P. furiosus*, with genes color-coded according to transcriptome fold changes. (C) Gene set enrichment analysis of archaeal clusters of orthologous genes (arCOGs), with significance levels indicated by a color bar ranging from white to dark purple. Genes with a *P*-value <0.05 are considered significantly overrepresented and highlighted by a circle, with circle size reflecting the number of genes in the category. (D) Volcano plot showing $\log_2$-fold changes for CS 1 condition compared to the control condition, with the *y*-axis displaying significance. A cutoff value of adjusted *P*-value of 0.05 is indicated by a dashed line, and relevant genes are highlighted. (E) Functional enrichment analysis using arCOG descriptions; significance levels and the number of regulated genes are shown in the upper legend. (F) Overlap between strongly upregulated (dark green) and downregulated (dark brown) genes in HS 1 and CS 1 conditions; total gene numbers are shown in horizontal bar graphs, and comparison set numbers are displayed in vertical bar graphs. (G) Scatter plot comparing the $\log_2$-fold changes for HS 1 (*x*-axis) and CS 1 (*y*-axis), color-coded according to plotting density; fold change densities for each condition are displayed in the side density plots. (H) TPM normalized expression values from the control condition for respective regulatory groups from panels A and D for CS 1 and HS 1 conditions; box edges delineate the first and third quartiles, center line represents the median, and whiskers denote points within 1.5× of the interquartile range.

groups of regulated genes of the HS and CS response was limited, except for the shared downregulation of amino acid metabolism (category E).

To further investigate this, we compared the gene-specific regulation of groups that are highly up- or downregulated under both conditions (Fig. 2F). A considerable proportion of genes downregulated during CS (41%) were also downregulated under HS. Similarly, this pattern was consistent for upregulated genes with 33% of the genes being upregulated during HS (Fig. S2 at https://doi.org/10.6084/m9.figshare.24006960.v1). Two currently uncharacterized transcription factors were upregulated under both CS and HS, suggesting either a potential general role in stress regulation or temperature-induced secondary effects that lead to the observed overlap between conditions (Fig. 2G). While the riboflavin operon remained unaffected during HS, the tungsten transport protein WtpA was substantially downregulated under HS and CS conditions. Comparing the expression levels of the control condition for the regulation group, we observed that HS triggered extensive reprogramming of the transcriptome (Fig. 2H). Initially, low transcribed genes are highly upregulated, while genes highly transcribed during exponential growth are massively downregulated (Fig. S3 at https://doi.org/10.6084/m9.figshare.24006960.v1). This pattern was not observed in the CS response, where only a smaller proportion of highly upregulated genes had lower expression values in the starting condition.

The results validate functional aspects of HS regulation and reveal some overlap with the CS response, warranting further investigation into the temporal dynamics of the thermal stress responses and the crosstalk of stress response pathways in general.

Temporal dynamics of the thermal stress response at the transcriptome level

We examined the number of up- and downregulated genes across all conditions, including HS 1, HS 2, and the recovery sample, using the previously established significance and fold change cutoffs (Fig. 3A). Approximately half of the strongly induced genes remained highly upregulated, while the other half returned to unchanged or mildly induced levels compared to the control sample. Minimal to no overlap with downregulated transcripts was observed, confirming the specificity of the response. This pattern also applied to normally upregulated genes, which returned to initial levels. A similar pattern emerged for downregulated genes although a higher proportion of initially downregulated genes became upregulated later. Samples taken 5 min after switching from HS or CS to recovery exhibited the lowest proportion of gene expression change, with only 4% being strongly up- or downregulated.

Gene enrichment analysis revealed a counter-regulation indicating a rapid recovery response for some cellular processes. Genes with transcription (category K) and replication (category L) annotations were overrepresented in the upregulated groups, but this pattern was not observed in the prolonged HS 2 condition, suggesting that extended heat exposure elicits a distinct response (Fig. 3B). Instead, translation-related genes (category J) are overrepresented after extended heat exposure, indicating a switch from protection to maintaining translation. Additionally, cell motility (category N) was induced and remained enriched even after recovery, alongside energy production (category C), which is overrepresented in downregulated genes at HS 1 and HS 2. Defense mechanisms (category V) were shut down during the immediate HS response. Notably, many currently uncharacterized genes (category R,S) were either shut down or upregulated during HS 1 and HS 2.

In the CS response, the number of highly up- or downregulated genes remained consistently low across all CS conditions (Fig. 3C). CS 1 and CS 2 exhibited a similar time-dynamic pattern as HS, with minimal to no overlap between up- and downregulated genes. In contrast, the 24-h response (CS 3) showed slightly more overlap between groups, with some genes that are not differently expressed after 2 h (CS 2) but altered after 24 h. However, a set of highly upregulated genes remained upregulated. Interestingly, the recovery condition displayed the most significant changes. As we hypothesized that this condition could induce a heat-shock-like reaction, we compared the results to a

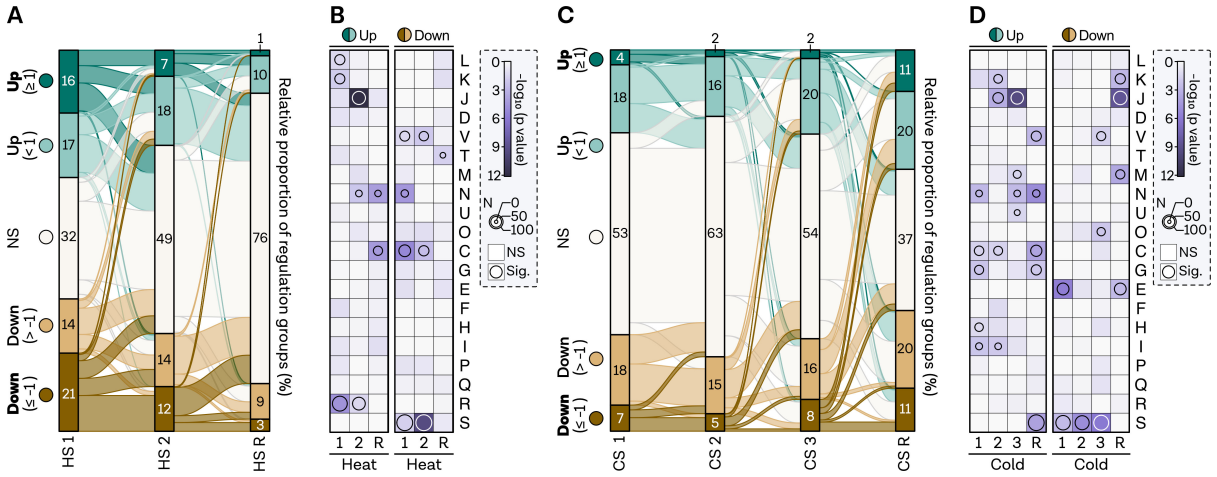

FIG 3 Temporal analysis shows rapid rebalancing of transcriptome changes following heat shock, while cold shock elicits multiple responses. (A) Flow diagram visualizing the relative number and interconnected genes between conditions (*x*-axis) in the HS experiment for each regulatory group: strongly upregulated (dark green, bold font), upregulated (light green), non-regulated (white), strongly downregulated (dark brown, bold font), and downregulated (light brown). The flow diagram size is plotted to scale. Note that due to rounding of the percentages to the nearest whole number, some values might not add up to 100%. (B) Gene set enrichment analysis of archaeal clusters of orthologous genes (arCOGs) for all three HS conditions. Significance levels are indicated by a continuous color bar from white to dark purple. Genes with a *P*-value <0.05 are considered significantly overrepresented and highlighted by a circle, with circle size reflecting the number of genes in the category. For better comparison, up and down categories include all upregulated and downregulated genes, respectively, regardless of fold changes. (C) Flow diagram for the CS experiment displaying the relative number and interconnected genes between conditions (*x*-axis) for each regulatory group, as described in panel A. The flow diagram size is plotted to scale. Note that due to rounding of the percentages to the nearest whole number, some values might not add up to 100%. (D) Gene set enrichment analysis of arCOGs for all four CS conditions, with significance levels indicated by a continuous color bar from white to dark purple. Genes with a *P*-value <0.05 are considered significantly overrepresented and highlighted by a circle, with circle size reflecting the number of genes in the category. For better comparison, up and down categories include all upregulated and downregulated genes, respectively, regardless of fold changes.

study using an HS setup from 90° to 97°, finding the best correlation to the CS recovery from all of the conditions (Fig. S4 at https://doi.org/10.6084/m9.figshare.24006960.v1) (78).

To further investigate this, we conducted functional enrichment analysis. Energy-related categories (category C, G) were overrepresented in almost all upregulated CS conditions, including recovery. Translation-related genes (category J) exhibited a delayed response in both HS and CS but were immediately counter-regulated in the CS recovery. Transcription (category K) was overrepresented in upregulated genes earlier than translation. In contrast, most downregulated genes in the CS response have not yet been described (category S). Only amino acid transport (category E) appears to be silenced, while the rest of the response is nonspecific.

In summary, differential gene expression and functional enrichment analysis of the RNA-seq data indicate that HS triggers substantial transcriptome changes, which is balanced remarkably quickly. In contrast, CS induces multiple responses, especially after a prolonged incubation time.

Investigating basal features of the archaeal transcriptome landscape in heat shock and cold shock regulation

Next, we investigated whether stress-induced genes share similar regulatory sequence features with genes under normal expression, highlighting their potential role in essential cellular functions. We first examined promoter elements, which have been shown to contribute to gene expression, although escape of the transcription elongation complex has been found to be the rate-limiting step during exponential growth (74). In *P. furiosus*, genes with archaea-typical BRE-TATA promoters display higher expression levels during exponential growth (Fig. 4A and B) (47). To determine whether stress-regulated

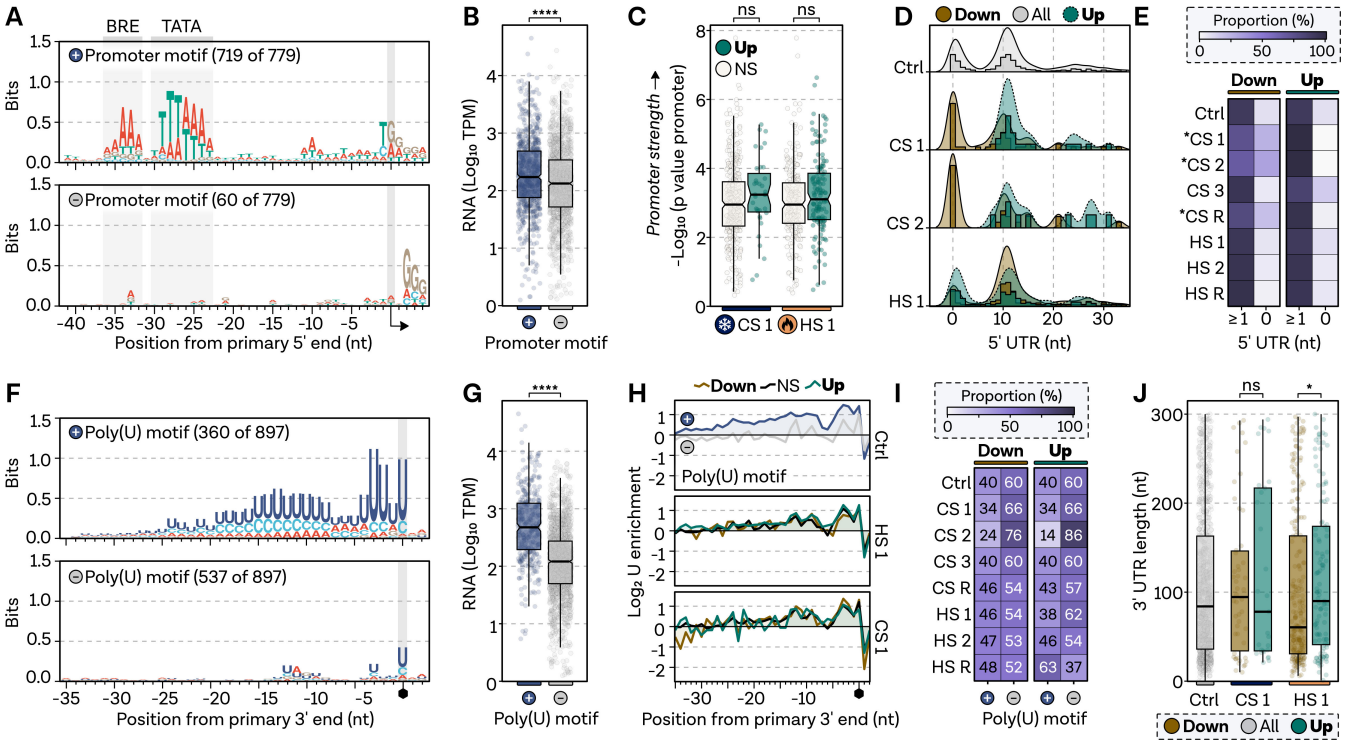

FIG 4 Stress-induced genes are equipped with archaea-typical regulatory sequences features. (A) Position-specific promoter motifs of primary transcripts from (47), grouped by MEME motif search into classical archaeal promoter motif or not, based on the presence of BRE and TATA elements. (B) Transcript abundance (TPM-normalized counts under control conditions) for genes with a promoter motif (blue) and without (gray). Box edges delineate first and third quartiles, center line represents median, and whiskers indicate points within 1.5× interquartile range. Welch's *t*-test used to assess differences between groups; significance level **** indicates *P*-values <0.0001. (C) Promoter strength comparison, estimated by *P*-values of MEME-detected promoter motifs (mode: one occurrence per site), for highly upregulated (dark green) and unchanged (white) genes under CS 1 and HS 1. Box plot parameters as in B; ns signifies *P*-values ≥0.05. (D) 5′ UTR length comparison for highly upregulated or downregulated genes against total distribution (Ctrl, 779). Density plots shown with bars in a window size of 1 and overlaid densities. (E) Proportion of leaderless (5′ UTR = 0) and leadered (5′ UTR ≥1) transcripts in highly upregulated and downregulated groups across all conditions. Chi-square test compares each stress condition to Ctrl sample distribution. Relative proportion color-coded from white (0) to dark purple (100%); significance (*P* < 0.05) indicated by an asterisk. (F) Position-specific terminator motif based on primary 3′ ends derived from Term-seq experiments, grouped by MEME search for genes with poly(U) signal (blue) or not (white). (G) Transcript abundance (TPM-normalized counts under control conditions) for genes with terminator poly(U) motif (blue) and without (gray). Box plot parameters as in B; significance level **** indicates *P*-values <0.0001. (H) Nucleotide enrichment meta-analysis compares nucleotide content of each group in a position-specific manner to randomly selected intergenic positions (n = 100,000). Log_2 enrichment shown for all primary 3′ ends with poly(U) motif (blue) or not (gray), and highly upregulated and downregulated genes in HS 1 and CS 1. (I) Proportion comparison of genes in regulatory groups with poly(U) signal or not, for all conditions. Note that an insufficient number of genes was detected for the CS 2 sample for robust statistical testing. Chi-square test checks whether the proportion of genes with poly(U) terminator differs significantly from Ctrl condition; no significant difference at *P* <0.05. (J) 3′ UTR comparison of regulatory groups to the Ctrl condition. Box plot parameters as in B; significance levels of * and ns indicate *P*-values <0.05 and ≥0.05, respectively.

genes are equipped with strong promoters, we analyzed the promoter strength of HS 1- and CS 1-induced genes, finding no difference compared to non-differential expressed genes (Fig. 4C). Notably, highly upregulated genes under CS conditions are all leadered, with a 5′ UTR of at least nine nucleotides possibly allowing efficient loading of the ribosome (Fig. 4D). Accordingly, more genes which are downregulated during CS are leaderless, which is significant in CS 1, CS 2, and the recovery condition (Fig. 4E).

Next, we employed Term-seq to survey the termination landscape of the *P. furiosus* transcriptome, identifying 897 enriched 3′ ends downstream of protein-coding transcripts under exponential growth conditions (Table S2 at https://doi.org/10.6084/m9.figshare.24007026.v1). In agreement with previous findings for archaea, we discovered a long poly(U)-stretch of approximately 16 bases enriched at the 3′ end (Fig. 4F) (75, 85). Although many genes (538 of 897) lack a robust poly(U)-signal, termination

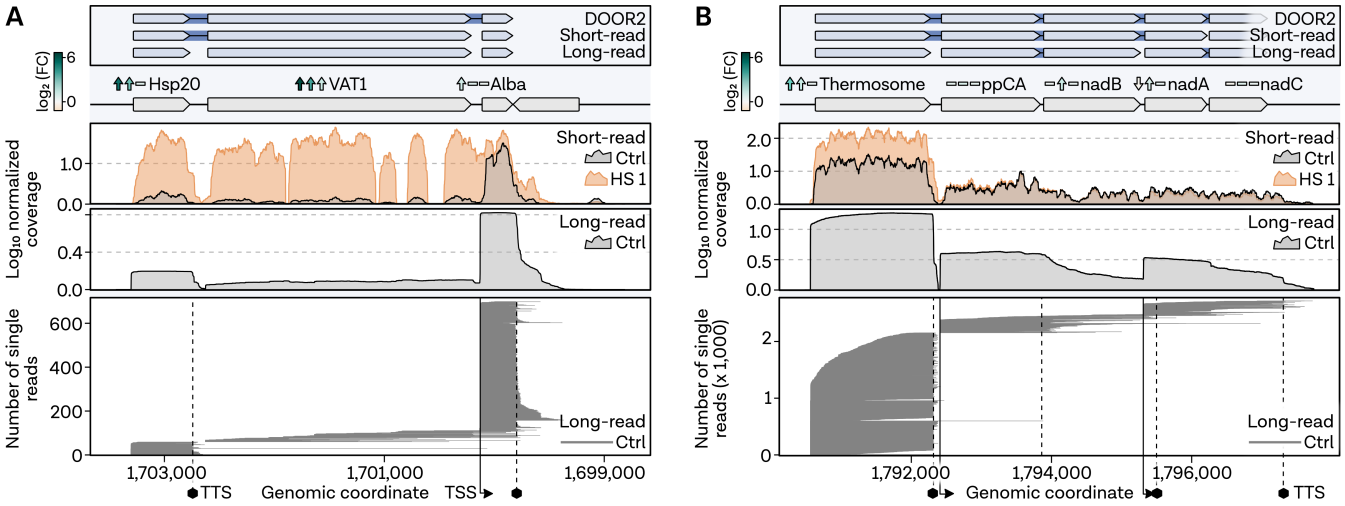

FIG 5 Long-read sequencing reveals operon organization of heat shock genes. (A) Operon analysis using long-read PCR-cDNA Nanopore sequencing for HSP20 operon and (B) thermosome operon. Top panel: annotated operons from DOOR2 database, previous short-read RNA-sequencing, and long-read Ctrl condition sequencing. Genes visualized as rectangles, strand indicated by arrow direction, and operons connected by blue background lines. Next panel: current gene annotation and log_2-fold changes on RNA level for three HS conditions (1, 2, R) from left to right. Significance indicated by up or down arrows. Profiles of mean normalized coverage values from Nanopore and short-read RNA-sequencing, color-coded as Ctrl (gray) and HS 1 (orange). The last panel presents a single-read analysis of Nanopore reads. Each line represents one full-length sequenced read, sorted by their read start position. Vertical lines indicate primary start sites identified in reference (47), while dashed lines represent primary 3′ ends from short-read Term-sequencing.

generally does not appear to be triggered by secondary structures (Fig. S5 at https://doi.org/10.6084/m9.figshare.24006960.v1). Genes exhibiting a strong poly(U)-motif at the 3′ end are highly expressed under optimal exponential growth conditions (Fig. 4G). Assessment of poly(U) enrichment in highly up- and downregulated genes under HS and CS conditions revealed no difference compared to the control sample, suggesting that numerous stress genes are terminated by poly(U)-signals and, therefore, equipped for efficient termination (Fig. 4H and I). Additionally, no difference in 3′ UTRs was observed between up- or downregulated genes in any condition except HS 1, where downregulated genes exhibit significantly shorter 3′ UTRs (Fig. 4J). Many genes associated with HS and CS in *P. furiosus* are predicted or validated to be transcribed within an operon, impacting transcriptional and translational regulation (47). Upon investigation of the operon organization of certain signature HS response genes, we found that the differential gene expression data did not correspond with operonization (Fig. 5A and B). To better understand the transcription of these genes, we collected long-read RNA-seq data using Nanopore sequencing of PCR-amplified cDNAs from the control condition. We specifically investigated an operon containing HSP20, VAT1, and the highly abundant DNA-binding protein AlbA. Single-read analysis confirmed 3′ end data gathered from Term-seq and primary 5′ end positions, suggesting a primary stop immediately after HSP20 and separate transcription start sites for each gene (Fig. 5A). This is consistent with Phr regulation of HSP20 and VAT1, as binding sites precede each gene. Interestingly, the stress condition HS 1 explains why the algorithm used in the 2019 paper, based on short-read data analysis of mixed RNA conditions, identified both of these genes in an operon (47). This observation is further supported when examining the thermosome operon, which, according to the long-read data, is distinctly transcribed as a single gene with very minimal readthrough rather than alongside other genes as annotated in the DOOR2 database (Fig. 5B).

Integrated transcriptomics and proteomics unveil shared functional responses and moderate correlation between total RNA and protein expression values

To further elucidate the molecular mechanisms underlying thermal stress response, we next analyzed the proteomics data (quantities and iBAQ values listed in Table S3 at https://doi.org/10.6084/m9.figshare.24007029.v1). Focusing on the HS response, where we observed a distinct response in the PCA (Fig. 1G), we identified 23% of the genes as upregulated and 26% as downregulated (Fig. 6A). Notably, $\log_2$-fold changes at the protein level were smaller as compared to the RNA level, prompting us to forgo applying an additional threshold for group description to ensure robust analysis. Key HS response proteins, such as the Myo-Synthase and Hsp20, displayed significant upregulation. Time-dependent analysis revealed no overlap between up- and downregulated groups during HS, a trend more pronounced than in the transcriptomics data. Moreover,

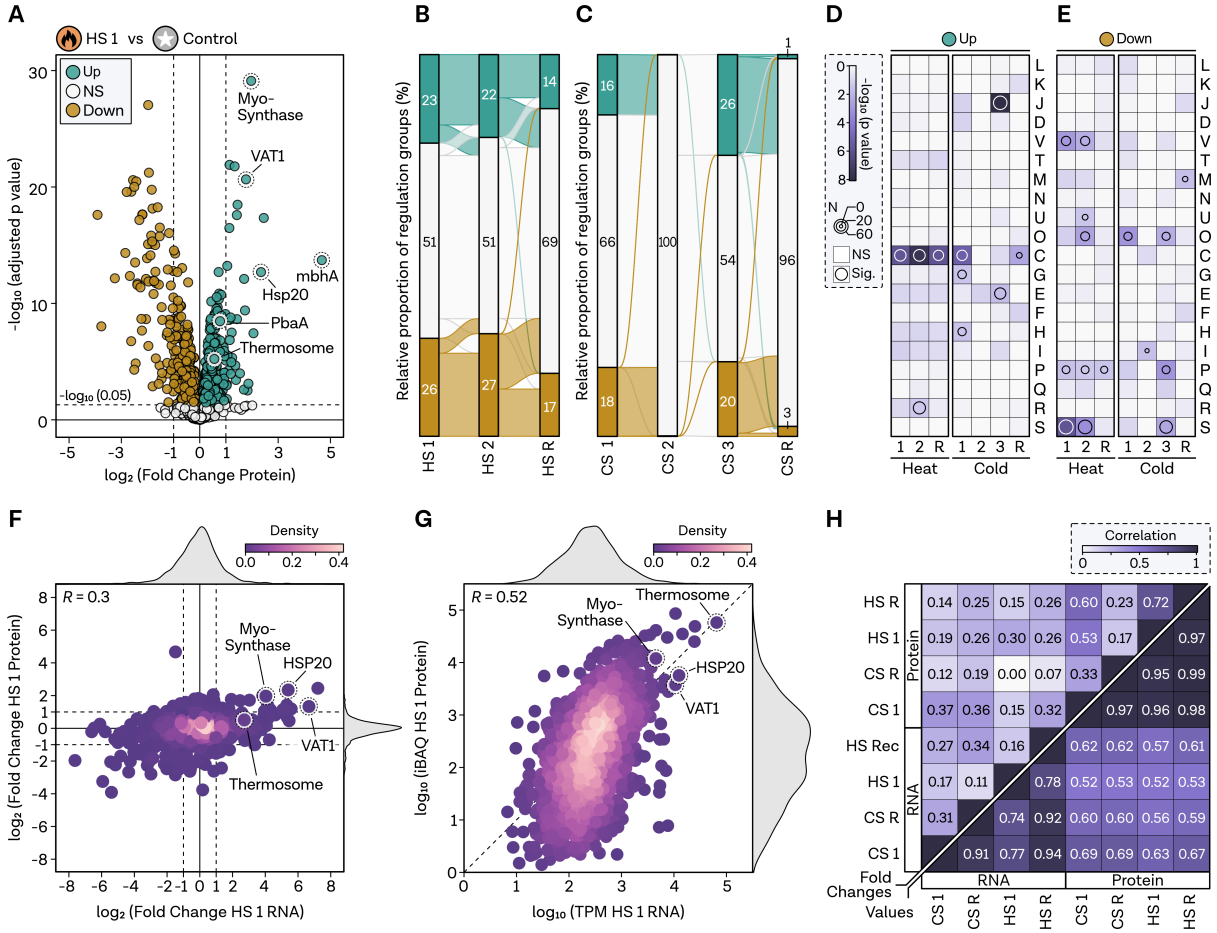

FIG 6 Proteomics count values but not fold changes are moderatly correlated to RNA levels. (A) Volcano plot displaying $\log_2$-fold changes in protein levels (*x*-axis) and −log10 (adjusted *P*-value, padj) on the *y*-axis comparing HS 1 (5 min) with control condition. Protein-coding genes are categorized based on significance and fold changes, color-coded as upregulated (padj < 0.05, $\log_2$FC > 0, green), non-regulated (NS, padj ≥ 0.05, white), and downregulated (padj < 0.05 and $\log_2$FC < 0, brown). HS genes are highlighted. Genes were assessed at a significance level of 0.05, indicated by a dashed line in the plot. (B) HS and (C) CS flow diagram visualizing the relative number and interconnected genes between conditions on the *x*-axis for each regulatory group, as described in panel A. Note that due to rounding of the percentages to the nearest whole number, some values might not add up to 100%. (D) Gene set enrichment analysis of archaeal clusters of orthologous genes (arCOGs) for all three HS and (E) all four CS conditions. Significance level is indicated by a continuous color bar from white to dark purple. Genes with a *P*-value <0.05 are considered significantly overrepresented in the category and are highlighted by a circle. The circle size reflects the number of genes in the category. (F) Comparison of $\log_2$-fold changes and (G) normalized TPM and iBAQ values of HS 1 measured at RNA (*x*-axis) and protein (*y*-axis) levels. HS genes are highlighted. Pearson's correlation coefficient is shown in the top left. Density of plotting is color-coded. (H) Correlation matrix (Pearson's correlation coefficient) of pairwise comparisons based on fold changes (upper left corner) and normalized count values (bottom right).

a larger number of proteins remained affected during the recovery condition compared to the RNA-seq data, indicating that protein-level reactions occur at a slower pace (Fig. 6B). For CS, we observed that 16% of proteins were upregulated after 20 min and 18% were downregulated, with virtually no change between the control condition and the 2 h protein sample (Fig. 6C). After 24 h, substantial alterations in the proteome were evident, with regulation rapidly reverting in the recovery sample.

Functional enrichment analysis demonstrated that overrepresented groups exhibited greater consistency compared to the RNA sequencing data (Fig. 6D). Energy-related genes (category C) were overrepresented across all upregulated HS categories, as well as in the CS 1 and recovery conditions, suggesting potential similarities at the protein level. Additionally, after 24 h of CS, translation-related genes (category J) were overrepresented, which had already been observed at the RNA level. Downregulated genes under HS included defense mechanisms (category V), ion transport (category P), and, in part, post-transcriptional modifications and chaperones (category O). Numerous currently uncharacterized proteins (category S) were also downregulated under HS (Fig. 6E).

Integrating our findings with the transcriptomics data, we identified a low correlation between fold changes; however, the same trend was evident for previously known HS-responsive genes (Fig. 6F). The correlation improved but remained moderate when comparing total expression values, normalized by either TPM for transcripts or iBAQ value for proteins (Fig. 6G). Upon comparing various conditions, we determined that the correlation between CS conditions was generally higher, particularly at the count level, where a notable correlation of 0.69 emerged between RNA and protein iBAQ values in CS 1 (Fig. 6H).

Identifying signature genes and common principles for heat shock and cold shock response

Analyzing the response regulated by the TF Phr in *P. furiosus*, we observed a time-dependent trend in RNA and protein values relative to the control sample, indicating a rapid transcriptome-level response followed by a more prolonged, less dynamic response at the protein level (Fig. 7A and B). To further examine regulatory aspects, we conducted a cluster analysis to identify groups sharing temporal trends in transcript and protein levels (summary of all data listed in Table S4 at https://doi.org/10.6084/m9.figshare.24007035.v1). Therefore, we performed hierarchical clustering of *z*-score normalized $\log_2$-fold changes, accounting for the varying sensitivities of RNA-seq and MS (Fig. 7C). In the HS response, we identified distinct clusters displaying either similar (cluster 3, 4) or contrasting trends in RNA and protein levels, particularly during HS 1 (cluster 1, 2) and HS 2 (cluster 5). Log_2-fold change analysis and arCOG enrichment of these clusters facilitated the integrative analysis in a functional context (Fig. 7D through F).

HS cluster 1 featured DNA maintenance and repair genes upregulated at the RNA level but downregulated at the protein level during HS 1, such as the cell cycle regulator cdc6, the DNA polymerase subunit B, the histone A2 (PF1722), and Hef-associated nucleases PF0399 and PF2015. Conversely, HS cluster 2 displayed counter-regulation, with upregulation of protein levels and downregulation of RNA levels. This cluster was significantly enriched in genes associated with central metabolism and translation-related processes. HS cluster 3 exhibited striking consistency in regulation, with genes related to post-translational modification, protein turnover, and chaperones initially downregulated during the immediate shock and subsequently recovering. This pattern was particularly evident for redox enzymes like SufB, SufC, and SufD. HS cluster 4 displayed the regulation expected for an HS protective response and is characterized by genes rapidly upregulated under HS 1 at the RNA level and a prolonged upregulating effect on the protein level. In this case, the signature genes were not selected based on arCOGs but on experimentally identified Phr targets, all of which were present in this cluster. However, while some transcription-related genes are overrepresented in cluster 4, we did not find some of the genes initially thought to contribute to thermal

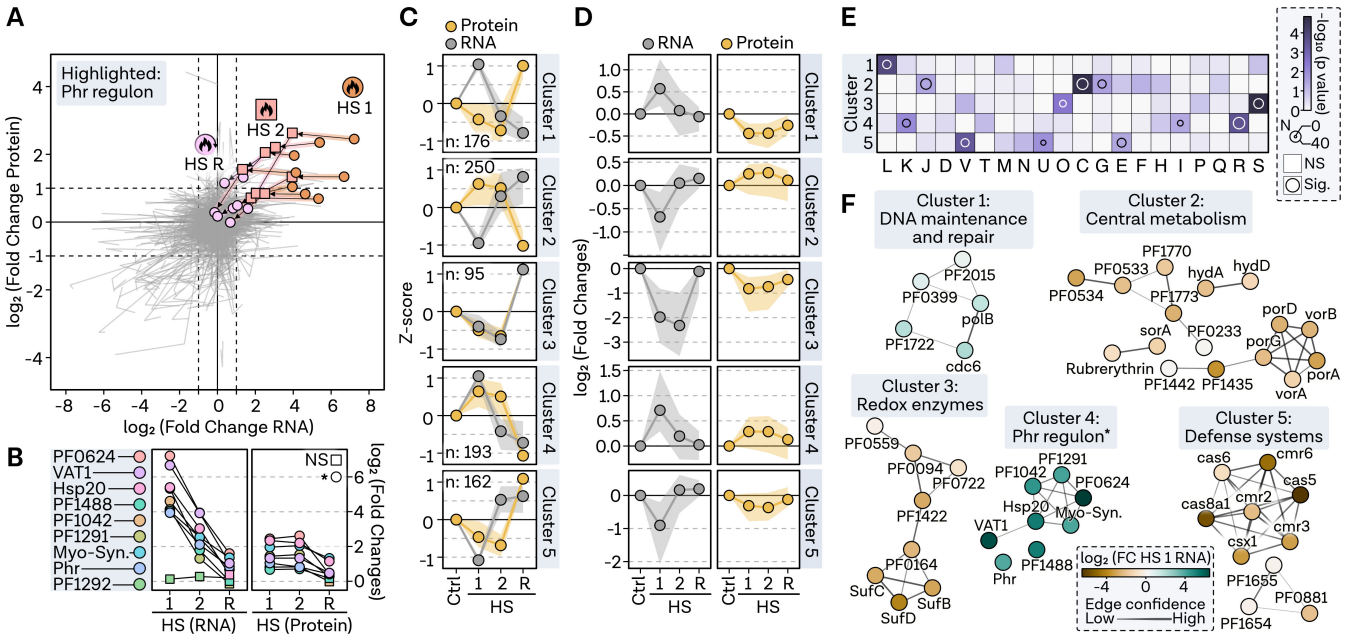

FIG 7 Cluster analysis identifies signature genes involved in heat shock response. (A) Pathway plot illustrating log_2-fold changes at RNA level (*x*-axis) and protein level (*y*-axis) in a line plot from condition HS 1 via HS 2 to recovery condition. Genes of the Phr regulon are highlighted with colors and points. (B) Fold changes for genes presented in panel A. Significant regulation in respective conditions is indicated by a circle (padj < 0.05) or a rectangle. (C) Comparison of median *z*-score values shown as a point in each cluster (row) and condition (column) for protein (yellow) and RNA (gray) values. Shaded area represents the interquartile range. (D) Log_2-fold changes of genes sorted by clusters. Points indicate median, while shaded area shows interquartile range. (E) Gene set enrichment analysis of archaeal clusters of orthologous genes (arCOGs) for five selected clusters. Significance level is represented by a continuous color bar from white to dark purple. Genes with a *P*-value <0.05 are considered significantly overrepresented in the category and are highlighted by a circle. Circle size reflects the number of genes in the category. (F) Functional enrichment analysis of genes from each cluster was performed by selecting all significantly regulated genes in the most significantly overrepresented arCOG category. Confidence in predicted interactions, according to the STRING database, is indicated by line thickness. Only genes with at least one connection are shown. Genes are depicted as points and colored based on the fold change at RNA level in condition HS 1.

fitness in the cluster. One prominent example are nucleoid-associated proteins (NAPs), like AlbA (PF1881), TrmBL2 (PF0496), and histones A1 (PF1831) and A2 (PF1722), that are not uniformly regulated (Fig. S6A at https://doi.org/10.6084/m9.figshare.24006960.v1). Nevertheless, we could confirm that *P. furiosus* has a high investment of the total protein to the NAPs, especially histone A2 and AlbA with protein levels increasing up to >5% under HS conditions (Fig. S6B at https://doi.org/10.6084/m9.figshare.24006960.v1) (17). Lastly, cluster 5 encompassed defense systems downregulated at the RNA level during HS 1, with protein levels remaining down for an extended period, displaying an opposite trend to cluster 4. This cluster contained genes related to defense systems transcribed from the Cas locus 1, including Cmr (Type III-B) and Cst (Type I-G), as well as transporter-related genes.

Re-evaluating the genes in HS cluster 4, we hypothesized that the Phr regulon may encompass additional targets not yet identified experimentally. Indeed, through motif analysis and comparison to the RegPrecise database, which houses transcriptional regulons based on comparative genomics, we discovered additional targets with palindromic Phr binding motifs, expanding the initial 10-gene group (Fig. S7 at https://doi.org/10.6084/m9.figshare.24006960.v1) (86). We identified the proteasome-assembling chaperone PbaA and its complex partner PF0014, the predicted transcriptional regulator PF1932, and the KaiC domain-containing protein PF1931 as additional targets strongly upregulated under HS (Fig. S7A and B at https://doi.org/10.6084/m9.figshare.24006960.v1). By comparing the Phr motif with the upstream sequences of predicted targets, we noted that genes predicted to have a motif but not exhibiting the typical Phr-mediated response at the RNA and protein levels, such as PF0239

and PF1117, deviate from the consensus sequence (Fig. S7C at https://doi.org/10.6084/m9.figshare.24006960.v1). Additionally, we confirmed previous analyses showing that PF0321 has two start sites, with only the more distant site being under the control of the Phr motif, resulting in a weaker response.

In analyzing the regulatory dynamics during CS response, we observed distinct short- and long-term responses, which were further investigated. Interestingly, the riboflavin operon and several highly upregulated genes during CS 1 were also affected at the protein level but were strongly downregulated during CS 1, while protein levels remained unchanged or even increased (Fig. 8A and B). Performing cluster analysis similar to the HS samples, we identified distinct clusters that are discussed in the following (Fig. 8C and D):

CS cluster 1 featured proteins especially upregulated at CS 3, with increasing upregulation at the RNA level over time, encompassing translation-related and membrane proteins (Fig. 8D through F). Notably, ribosomal proteins were upregulated at the protein level after 24 h, counter-regulated after recovery at 95°C. Interestingly, PF1265, a tRNA/rRNA cytosine-C5 methylase, was identified in this cluster. Further analysis of potential tRNA/rRNA-modifying genes revealed that PF1265 was, indeed, the only gene upregulated under CS 3 at both RNA and protein levels (Fig. S8 at https://doi.org/10.6084/m9.figshare.24006960.v1). Conversely, KsgA expression was downregulated at the protein level after HS, and only the Fmu homolog PF0666 and the tRNA methyltransferase PF1871 were upregulated at both levels during HS. CS cluster 2 is characterized by coordinated downregulation at both RNA and protein levels, particularly after prolonged CS. This cluster contains several unknown genes, as well as

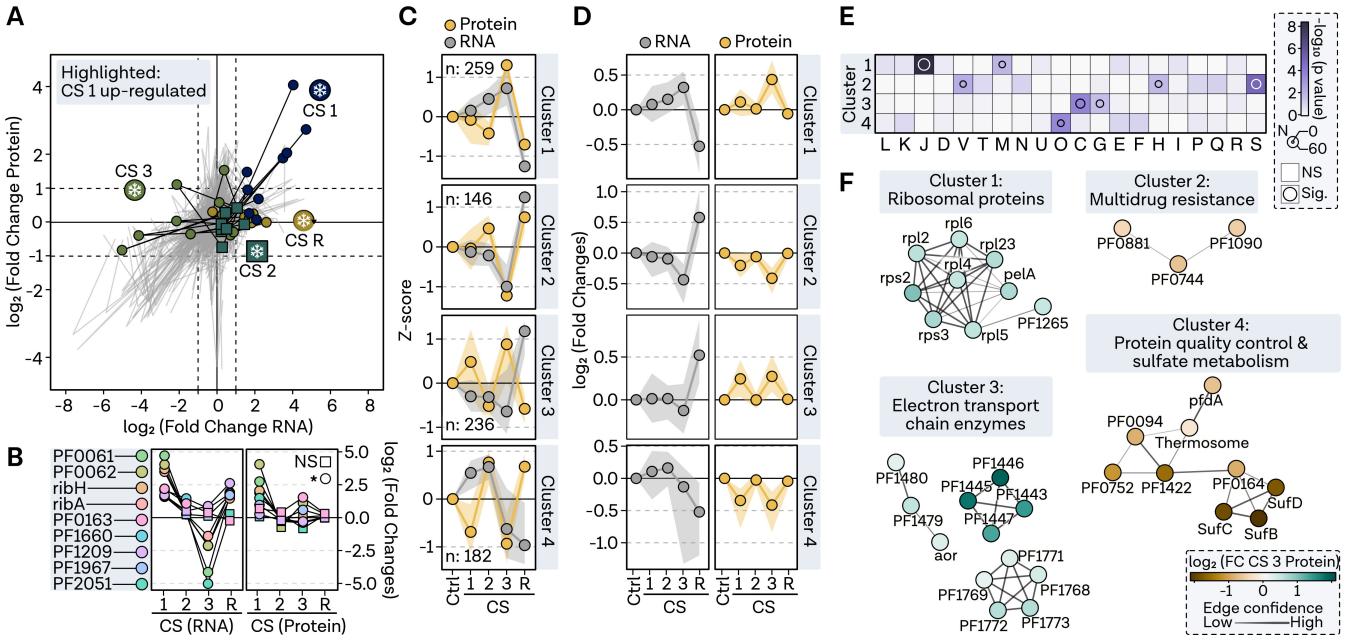

FIG 8 Cluster analysis identifies signature genes involved in cold shock response. (A) Pathway plot illustrating log_2-fold changes at RNA level (*x*-axis) and protein level (*y*-axis) in a line plot from condition CS 1, through CS 2 and CS 3 to recovery condition. The nine genes with the highest upregulation at RNA level (CS 1) are highlighted with colors and points. (B) Fold changes for genes presented in panel G. Significant regulation in respective conditions is indicated by a circle (padj < 0.05) or a rectangle. (C), Comparison of median *Z*-score values shown as a point in each cluster (row) and condition (column) for protein (yellow) and RNA (gray) values. Shaded area represents the interquartile range. (D) Log_2-fold changes of genes sorted by clusters. Points indicate median, while shaded area shows interquartile range. (E) Gene set enrichment analysis of archaeal clusters of orthologous genes (arCOGs) for four selected clusters. Significance level is represented by a continuous color bar from white to dark purple. Genes with a *P*-value <0.05 are considered significantly overrepresented in the category and are highlighted by a circle. Circle size reflects the number of genes in the category. (F) Functional enrichment analysis of genes from each cluster was performed by selecting all significantly regulated genes in the most significantly overrepresented arCOG category. Confidence in predicted interactions, according to the STRING database, is indicated by line thickness. Only genes with at least one connection are shown. Genes are depicted as points and colored based on the fold change at protein level in condition CS 3.

transporters related to multidrug resistance. CS cluster 3 exhibits upregulation at CS 1 and CS 3 time points on the protein level and is enriched in metabolism-related genes, including electron transport chain enzymes. In contrast, CS cluster 4 displays downregulation at the protein level immediately following CS. Interestingly, this cluster contains proteins involved in protein quality control, such as the thermosome and prefoldin alpha, and Fe-S cluster assembly proteins SufB, SufC, and SufD, which are implicated in sulfate metabolism.

Considering that some of these genes are regulated by the TF SurR (PF0095), we investigated the overlap between the thermal stress response to other known TF-regulons in *P. furiosus*. Therefore, we examined experimentally verified regulons, such as SurR, CopR (PF0739), TrmBL1 (PF0124), TFB-RF1 (PF1088), as well as predicted regulons like cobalamin biosynthesis regulation by CblrR (unknown), riboflavin biosynthesis operon regulation by RbkR (PF0988), and thiamin transport regulation by ThiR (PF0601) (Fig. S9 at https://doi.org/10.6084/m9.figshare.24006960.v1) (40, 86–90). Many genes controlled by validated or yet unknown transcription factors exhibit significant regulation at both the RNA and protein levels, suggesting either TF regulatory networks that affect one another or secondary effects. While genes upregulated by SurR during the primary S^0 response also exhibit upregulation under CS and HS, genes downregulated by SurR display consistent downregulation under the tested conditions at the RNA level. Intriguingly, targets of the copper-regulator CopR are substantially downregulated, especially genes involved in binding and transporting metal ions, such as PF0723.

To explore additional possible determinants of RNA and protein fate, we analyzed sequence features, including the codon adaptation index (CAI) and GC content of coding regions (Summary of all data listed in Table S4 at https://doi.org/10.6084/m9.figshare.24007035.v1) (Fig. S10 at https://doi.org/10.6084/m9.figshare.24006960.v1). We found that all HS clusters characterized by upregulation of the proteome (clusters 2 and 4) exhibit significantly higher CAI values compared to the overall distribution (Fig. S10A at https://doi.org/10.6084/m9.figshare.24006960.v1). Cluster 2 is also characterized by genes with higher GC content, while cluster 1 has lower than expected GC values (Fig. S10B at https://doi.org/10.6084/m9.figshare.24006960.v1). Regarding the CS clusters, not only do the clusters characterized by protein upregulation exhibit higher CAI values but also cluster 4. However, the GC content is only significantly higher in clusters 1 and 3 (Fig. S10C and D at https://doi.org/10.6084/m9.figshare.24006960.v1).

In summary, while the response to HS is regulated by Phr and possibly encoded at the sequence level, other effects are likely controlled by currently undetermined features, as well as post-transcriptional and post-translational regulatory mechanisms.

DISCUSSION

In this study, we investigated the response of the hyperthermophilic archaeon *P. furiosus* to HS and CS, unveiling complex patterns of gene expression and protein regulation. Our results indicate a coordinated, temporally organized response, utilizing various adaptive mechanisms for distinct cellular processes and pathways. Refined clustering and functional analysis provided a clear depiction of the various regulatory patterns observed in the HS and CS response of *P. furiosus*, highlighting the complexity of molecular mechanisms underlying this process. However, it is crucial to acknowledge that besides the direct response to temperature stress, the results may also include secondary effects induced by the temperature change itself. These could be influenced by various cellular processes, such as growth rate alterations or changes in energy utilization, that contribute to the overall transcriptional and proteomic landscape.

HS triggers extensive reprogramming of the transcriptome, upregulating numerous heat shock proteins that serve to prevent cellular damage. We confirmed HS-induced upregulation of predicted targets of the transcriptional regulator Phr on both RNA and protein levels in a time-resolved manner, thus broadening its known regulon (40). Moreover, we demonstrated that stress-induced genes generally possess archaea-typical promoter and transcription terminator sequences. This suggests that these genes are

silenced under normal growth conditions but can be rapidly activated, as observed for Phr-regulated genes. While HS primarily leads to the upregulation of proteins related to energy production and transcription-related processes, we observed the downregulation of defense mechanisms, including the CRISPR-Cas system. Silencing of these systems during stress might be attributed to energy conservation or preventing inadvertent activation of the immune response, which could adversely affect genome stability, especially since RNA and DNA targeting CRISPR-Cas systems coexist in *Pyrococcus* (91, 92).

While we and others found a number of proteins that confer a specific heat shock response, we did not identify proteins that confer protection against CS. The CS response appears to be characterized by two distinct phases: an initial phase focused on energy provision, followed by a phase aimed at sustaining translation. This coordinated response is evident at both RNA and protein levels and rapidly reverts during recovery. Regulation during CS is more subtle compared to HS, with multiple responses observed at both short- and longer-term CS on RNA and protein levels. While previous studies investigating the CS response in (hyper-)thermophilic archaea have identified some cold-induced genes, only a subset of these are reflected in our data. This discrepancy might be explained by the experimental conditions used in earlier studies, which primarily involved temperatures at the lower growth limit as the CS temperature (83, 93, 94). Nevertheless, a 4°C shock is a plausible scenario for these organisms, considering their exposure to surrounding cold seawater that may also penetrate the porous material of black smokers (95).

Interestingly, it has been reported that general adaptations of psychrophilic archaea share some characteristics with CS response in hyperthermophiles (94). One of these signature domains found in psychrophiles is TRAM, which is universally distributed and functions via RNA chaperone activity (96–98). The protein containing this domain, possibly mimicking the bacterial cold shock protein A function in archaea, is also present in *P. furiosus* (PF1062). While it is downregulated under early CS conditions, it is significantly upregulated after 24 h on the protein level. In addition to the investigation of single cold-induced genes, a global quantitative proteomics study in the cold-adapted *Methanococcoides burtonii* demonstrated that the abundance of ribosomal subunits peaked at 4°C (99). Our analysis supports this observation, as we detected a time-dependent upregulation of ribosomal proteins. Interestingly, this may be connected to the finding that genes upregulated during early CS in our study consistently possess a 5′ leader sequence, compared to approximately 15% leaderless genes observed under normal conditions. The presence of a 5′ leader sequence, including a Shine-Dalgarno site, could potentially facilitate ribosome recruitment and translation initiation factor binding, thereby ensuring efficient translation of cold-responsive genes under these challenging conditions (100). Moreover, this arrangement may allow for more intricate post-transcriptional regulatory mechanisms, such as RNA-binding protein interactions or secondary structure formation, which could enable fine-tuning of gene expression. However, the mechanism of leaderless translation remains unclear, complicating functional comparisons (101–103). Although it has been shown that this can be facilitated by 30S ribosomal subunits pre-loaded with initiator tRNA, it remains an open question whether this process is also influenced by additional ribosomal proteins (as observed in Bacteria) or if ribosome hetereogeneity, in general, plays a role (104–106). Interestingly, bacterial ribosome biogenesis has been shown to be coupled to post-translational protein quality control through the HSP70 machinery under stress conditions (107, 108). Furthermore, ribosome biogenesis, being an energy-demanding process sensitive to temperature fluctuations, may lead to an enrichment of distinct rRNA precursors under thermal stress conditions affecting ribosome composition (108–110).

Although previous research has indicated that ribosomal RNA transcription in *P. furiosus* is influenced by growth rate, temperature-dependent rRNA heterogeneity in *Thermococcales* has not been studied (111). The use of a recently established Nanopore protocol could enable temperature-dependent rRNA processing and simultaneously

identifying potential rRNA modifications that contribute to ribosome function (112). Some modifications, such as KsgA-dependent dimethylation and Nat10-dependent acetlyation, have already been shown to contribute to fitness and adaptation (68, 113). Notably, the extent of ac^4C acetylations is significantly increased in response to temperature increases in *Thermococcus* and *Pyrococcus*, with a stabilizing effect on the RNA (113). Understanding the functional implications of these modifications and their significance in ribosome dynamics under thermal stress warrants further exploration (114, 115).

Combining Nanopore approaches, enabling to tackle ribosome heterogeneity, with ribo-seq analysis at different temperatures would be a highly promising approach. Integrating these complementary techniques could offer valuable insights into ribosomal subpopulations and potential temperature-specific translation regulations, providing a more comprehensive understanding of adaptive stress response in hyperthermophilic archaea.

The overlap of transcription regulons examined in this study underscores the complex cellular responses to environmental stressors, which may be coordinated across a broad range of conditions. Notable examples include the RbkR-regulated riboflavin (vitamin B_2) operon, producing essential cofactor precursors flavin mononucleotide (FMN) and flavin adenine dinucleotide (FAD), and the ThiR-regulated thiamine (vitamin B_1) operon, precursor of thiamine pyrophosphate (TPP) (84, 116, 117). Given the substantial upregulation of energy-related enzymes during CS, there may be an increased demand for maintaining proper functioning of metabolic pathways, which could explain the upregulation of these operons (118). Alternatively, secondary effects may also contribute to the observed transcriptional regulation. For example, disrupted redox homeostasis might explain the regulation of SurR targets, which is a redox-active transcriptional regulator (87, 119, 120).

Although our study has yielded significant findings, we must acknowledge certain limitations. Our experimental design focused on specific time points, potentially missing the full dynamics of gene expression changes during stress response. Time-course experiments for certain targets would offer a more comprehensive view of temporal changes in gene expression and could reveal additional regulatory mechanisms. Additionally, our experimental setup allows only for relative quantitative comparisons of the final amounts of transcripts and proteins in the cell. As such, we cannot make definitive statements regarding the neo-synthesis of RNA and proteins, which should be considered for interpretation. Furthermore, we cannot address the heterogeneity of responses on the genome and transcriptome levels. While single-cell analysis has provided deeper insights into individual cellular mechanisms during thermal stress and various growth conditions in bacteria, its application to archaea remains unexplored (121, 122). Future utilization of single-cell technologies will help uncover rare cellular states and genome plasticity of individual *Pyrococcus furiosus* cells, particularly during HS, shedding light on the diverse strategies these organisms employ to cope with extreme environments.

In conclusion, our study comprehensively analyses the transcriptomic and proteomic responses to thermal stress in the hyperthermophilic archaeon *Pyrococcus furiosus*. We identified distinct expression patterns and regulatory mechanisms, providing valuable insights into the dynamic response mechanisms to environmental fluctuations and their control by transcription factor networks in archaea. Our findings enhance our understanding of *P. furiosus'* remarkable adaptability and expand our knowledge of life in extreme environments.

ACKNOWLEDGMENTS

We thank all the members of the Grohmann lab for fruitful discussions. H.U. and C.L. would like to acknowledge Lisa Neuenroth at the Department of Clinical Chemistry, University Medical Center Göttingen, for expert technical support of the mass spectro-

metric analyses. We, furthermore, would like to thank Eveline Peeters and Rani Baes for stimulating discussions and their expertise in archaeal biology.

Work in the Grohmann lab was supported by the Deutsche Forschungsgemeinschaft (DFG funding schemes SPP2141 "Much more than defence: the multiple functions and facets of CRISPR-Cas" and SFB960 TPA7 to D.G.). H.U. received funding via the DFG SPP2141 "Much more than defence: the multiple functions and facets of CRISPR-Cas".

AUTHOR AFFILIATIONS

[1]Institute of Biochemistry, Genetics and Microbiology, Institute of Microbiology and Archaea Centre, Single-Molecule Biochemistry Lab and Regensburg Center for Biochemistry, University of Regensburg, Regensburg, Germany
[2]Bioanalytical Mass Spectrometry Group, Max Planck Institute for Multidisciplinary Sciences, Göttingen, Germany
[3]Department of Clinical Chemistry, University Medical Center Göttingen, Göttingen, Germany

PRESENT ADDRESS

Georg Schmid, Microbify GmbH, Straubing, Germany
Martin Fenk, Max Planck Institute for Infection Biology, Berlin, Germany

AUTHOR ORCIDs

Felix Grünberger http://orcid.org/0000-0001-7444-2408
Zubeir El Ahmad http://orcid.org/0009-0005-6904-0208
Winfried Hausner http://orcid.org/0000-0002-4382-7468
Dina Grohmann http://orcid.org/0000-0002-0570-2517

FUNDING

Funder	Grant(s)	Author(s)
Deutsche Forschungsgemeinschaft (DFG)	SPP2141	Dina Grohmann
Deutsche Forschungsgemeinschaft (DFG)	SFB 960 / TP A7	Dina Grohmann
Deutsche Forschungsgemeinschaft (DFG)	SPP2141	Henning Urlaub

AUTHOR CONTRIBUTIONS

Felix Grünberger, Conceptualization, Data curation, Formal analysis, Investigation, Methodology, Validation, Visualization, Writing – original draft, Writing – review and editing | Georg Schmid, Investigation, Methodology | Zubeir El Ahmad, Data curation, Formal analysis, Investigation, Methodology, Writing – review and editing | Martin Fenk, Data curation, Formal analysis, Investigation, Methodology, Writing – review and editing | Katharina Vogl, Investigation | Robert Reichelt, Conceptualization, Methodology, Writing – review and editing | Winfried Hausner, Conceptualization, Methodology, Writing – review and editing | Henning Urlaub, Conceptualization, Funding acquisition, Methodology, Writing – review and editing | Christof Lenz, Conceptualization, Data curation, Investigation, Methodology, Supervision, Writing – review and editing | Dina Grohmann, Conceptualization, Funding acquisition, Project administration, Supervision, Writing – review and editing

DATA AVAILABILITY

RNA sequencing data are available at the European Nucleotide Archive (ENA, https://www.ebi.ac.uk/ena) under project accession numbers PRJEB61174 (RNA-seq data used for differential gene expression analysis) and PRJEB61177 (Term-seq and Nanopore data) (123).

The mass spectrometry proteomics data have been deposited to the ProteomeXchange Consortium via the PRIDE partner repository with the datasetdata set identifier PXD041262 (124).
Documentation and code of all essential analysis steps (tools and custom Rscripts) are available from https://github.com/felixgrunberger/HSCS_Pfu.

REFERENCES

1. Demirjian DC, Morís-Varas F, Cassidy CS. 2001. Enzymes from extremophiles. Curr Opin Chem Biol 5:144–151. https://doi.org/10.1016/s1367-5931(00)00183-6
2. Pikuta EV, Hoover RB, Tang J. 2007. Microbial extremophiles at the limits of life. Crit Rev Microbiol 33:183–209. https://doi.org/10.1080/10408410701451948
3. Stetter KO. 1999. Extremophiles and their adaptation to hot environments. FEBS Lett 452:22–25. https://doi.org/10.1016/s0014--5793(99)00663-8
4. Raddadi N, Cherif A, Daffonchio D, Neifar M, Fava F. 2015. Biotechnological applications of extremophiles, extremozymes and extremolytes. Appl Microbiol Biotechnol 99:7907–7913. https://doi.org/10.1007/s00253-015-6874-9
5. Laksanalamai P, Maeder DL, Robb FT. 2001. Regulation and mechanism of action of the small heat shock protein from the hyperthermophilic archaeon *Pyrococcus furiosus*. J Bacteriol 183:5198–5202. https://doi.org/10.1128/JB.183.17.5198-5202.2001
6. Poole FL, Gerwe BA, Hopkins RC, Schut GJ, Weinberg MV, Jenney FE, Adams MWW. 2005. Defining genes in the genome of the hyperthermophilic archaeon *Pyrococcus furiosus*. J Bacteriol 187:7325–7332. https://doi.org/10.1128/JB.187.21.7325-7332.2005
7. Shockley KR, Ward DE, Chhabra SR, Conners SB, Montero CI, Kelly RM. 2003. Heat shock response by the hyperthermophilic archaeon *Pyrococcus furiosus*. Appl Environ Microbiol 69:2365–2371. https://doi.org/10.1128/AEM.69.4.2365-2371.2003
8. Fiala G, Stetter KO. 1986. *Pyrococcus furiosus* sp. nov. represents a novel genus of marine heterotrophic archaebacteria growing optimally at 100°C. Arch. Microbiol 145:56–61. https://doi.org/10.1007/BF00413027
9. Zierenberg RA, Adams MW, Arp AJ. 2000. Life in extreme environments: hydrothermal vents. Proc Natl Acad Sci U S A 97:12961–12962. https://doi.org/10.1073/pnas.210395997
10. Teske A, Edgcomb V, Rivers AR, Thompson JR, de Vera Gomez A, Molyneaux SJ, Wirsen CO. 2009. A molecular and physiological survey of a diverse collection of hydrothermal vent *Thermococcus* and *Pyrococcus* isolates. Extremophiles 13:905–915. https://doi.org/10.1007/s00792-009-0278-7
11. Leston S, Nunes M, Rosa J, Lemos MFL, Ramos F, Pardal MA. 2014. Prospection, collection, and preservation of Marine samples, p 15–34. In In comprehensive Analytical chemistry. Elsevier
12. Wirth R. 2017. Colonization of black smokers by hyperthermophilic microorganisms. Trends Microbiol 25:92–99. https://doi.org/10.1016/j.tim.2016.11.002
13. Wirth R, Luckner M, Wanner G. 2018. Validation of a hypothesis: colonization of black smokers by hyperthermophilic microorganisms. Front Microbiol 9:524. https://doi.org/10.3389/fmicb.2018.00524
14. Huber R, Stotters P, Cheminee JL, Richnow HH, Stetter KO. 1990. Hyperthermophilic archaebacteria within the crater and open-sea plume of erupting MacDonald Seamount. Nature 345:179–182. https://doi.org/10.1038/345179a0
15. Mora M, Bellack A, Ugele M, Hopf J, Wirth R. 2014. The temperature gradient-forming device, an accessory unit for normal light microscopes to study the biology of hyperthermophilic microorganisms. Appl Environ Microbiol 80:4764–4770. https://doi.org/10.1128/AEM.00984-14
16. Hickey DA, Singer GA. 2004. Genomic and proteomic adaptations to growth at high temperature. Genome Biol 5:117. https://doi.org/10.1186/gb-2004-5-10-117
17. Hocher A, Borrel G, Fadhlaoui K, Brugère JF, Gribaldo S, Warnecke T. 2022. Growth temperature and chromatinization in archaea. Nat Microbiol 7:1932–1942. https://doi.org/10.1038/s41564-022-01245-2
18. Zeldovich KB, Berezovsky IN, Shakhnovich EI. 2007. Protein and DNA sequence determinants of thermophilic adaptation. PLoS Comput Biol 3:e5. https://doi.org/10.1371/journal.pcbi.0030005
19. Lipscomb GL, Hahn EM, Crowley AT, Adams MWW. 2017. Reverse gyrase is essential for microbial growth at 95°C. Extremophiles 21:603–608. https://doi.org/10.1007/s00792-017-0929-z
20. Kikuchi A, Asai K. 1984. Reverse gyrase--a topoisomerase which introduces positive superhelical turns into DNA. Nature 309:677–681. https://doi.org/10.1038/309677a0
21. Lemmens L, Baes R, Peeters E. 2018. Heat shock response in archaea. Emerg Top Life Sci 2:581–593. https://doi.org/10.1042/ETLS20180024
22. Richter K, Haslbeck M, Buchner J. 2010. The heat shock response: life on the verge of death. Mol Cell 40:253–266. https://doi.org/10.1016/j.molcel.2010.10.006
23. Cavicchioli R, Thomas T, Curmi PMG. 2000. Cold stress response in archaea. Extremophiles 4:321–331. https://doi.org/10.1007/s007920070001
24. Zhang Y, Gross CA. 2021. Cold shock response in bacteria. Annu Rev Genet 55:377–400. https://doi.org/10.1146/annurev-genet-071819-031654
25. Fields PA. 2001. Review: protein function at thermal extremes: balancing stability and flexibility. Comp Biochem Physiol A Mol Integr Physiol 129:417–431. https://doi.org/10.1016/s1095-6433(00)00359-7
26. Phadtare S, Severinov K. 2010. RNA remodeling and gene regulation by cold shock proteins. RNA Biol 7:788–795. https://doi.org/10.4161/rna.7.6.13482
27. Roncarati D, Scarlato V. 2017. Regulation of heat-shock genes in bacteria: from signal sensing to gene expression output. FEMS Microbiol Rev 41:549–574. https://doi.org/10.1093/femsre/fux015
28. Hu Y, Oliver HF, Raengpradub S, Palmer ME, Orsi RH, Wiedmann M, Boor KJ. 2007. Transcriptomic and phenotypic analyses suggest a network between the transcriptional regulators HrcA and σB in *Listeria monocytogenes*. Appl Environ Microbiol 73:7981–7991. https://doi.org/10.1128/AEM.01281-07
29. Narberhaus F. 1999. Negative regulation of bacterial heat shock genes. Mol Microbiol 31:1–8. https://doi.org/10.1046/j.1365-2958.1999.01166.x
30. Roncarati D, Pinatel E, Fiore E, Peano C, Loibman S, Scarlato V. 2019. *Helicobacter pylori* stress-response: definition of the HrcA regulon. Microorganisms 7:436. https://doi.org/10.3390/microorganisms7100436
31. Phadtare S. 2004. Recent developments in bacterial cold-shock response. Curr Issues Mol Biol 6:125–136.
32. Yamanaka K, Fang L, Inouye M. 1998. The CspA family in *Escherichia coli*: multiple gene duplication for stress adaptation. Mol Microbiol 27:247–255. https://doi.org/10.1046/j.1365-2958.1998.00683.x
33. Al-Fageeh MB, Smales CM. 2006. Control and regulation of the cellular responses to cold shock: the responses in yeast and mammalian systems. Biochem J 397:247–259. https://doi.org/10.1042/BJ20060166
34. Overgaard J, Sørensen JG, Petersen SO, Loeschcke V, Holmstrup M. 2005. Changes in membrane lipid composition following rapid cold hardening in *Drosophila melanogaster*. J Insect Physiol 51:1173–1182. https://doi.org/10.1016/j.jinsphys.2005.06.007
35. Shamovsky I, Nudler E. 2008. New insights into the mechanism of heat shock response activation. Cell Mol Life Sci 65:855–861. https://doi.org/10.1007/s00018-008-7458-y
36. West JD, Wang Y, Morano KA. 2012. Small molecule activators of the heat shock response: chemical properties, molecular targets, and therapeutic promise. Chem Res Toxicol 25:2036–2053. https://doi.org/10.1021/tx300264x

37. Giaquinto L, Curmi PMG, Siddiqui KS, Poljak A, DeLong E, DasSarma S, Cavicchioli R. 2007. Structure and function of cold shock proteins in archaea. J Bacteriol 189:5738–5748. https://doi.org/10.1128/JB.00395-07
38. Vierke G, Engelmann A, Hebbeln C, Thomm M. 2003. A novel archaeal transcriptional regulator of heat shock response. J Biol Chem 278:18–26. https://doi.org/10.1074/jbc.M209250200
39. Liu W, Vierke G, Wenke AK, Thomm M, Ladenstein R. 2007. Crystal structure of the archaeal heat shock regulator from *Pyrococcus furiosus*: a molecular chimera representing eukaryal and bacterial features. J Mol Biol 369:474–488. https://doi.org/10.1016/j.jmb.2007.03.044
40. Keese AM, Schut GJ, Ouhammouch M, Adams MWW, Thomm M. 2010. Genome-wide identification of targets for the archaeal heat shock regulator phr by cell-free transcription of genomic DNA. J Bacteriol 192:1292–1298. https://doi.org/10.1128/JB.00924-09
41. Baes R, Lemmens L, Mignon K, Carlier M, Peeters E. 2020. Defining heat shock response for the thermoacidophilic model crenarchaeon *Sulfolobus acidocaldarius*. Extremophiles 24:681–692. https://doi.org/10.1007/s00792-020-01184-y
42. Kagawa HK, Yaoi T, Brocchieri L, McMillan RA, Alton T, Trent JD. 2003. The composition, structure and stability of a group II chaperonin are temperature regulated in a hyperthermophilic archaeon. Mol Microbiol 48:143–156. https://doi.org/10.1046/j.1365-2958.2003.03418.x
43. Babski J, Maier LK, Heyer R, Jaschinski K, Prasse D, Jäger D, Randau L, Schmitz RA, Marchfelder A, Soppa J. 2014. Small regulatory RNAs in archaea. RNA Biol 11:484–493. https://doi.org/10.4161/rna.28452
44. Gelsinger DR, DiRuggiero J. 2018. Transcriptional landscape and regulatory roles of small noncoding RNAs in the oxidative stress response of the haloarchaeon *Haloferax volcanii*. J Bacteriol 200:e00779-17. https://doi.org/10.1128/JB.00779-17
45. Gomes-Filho JV, Daume M, Randau L. 2018. Unique archaeal small RNAs. Annu Rev Genet 52:465–487. https://doi.org/10.1146/annurev-genet-120417-031300
46. Lorenzetti APR, Kusebauch U, Zaramela LS, Wu WJ, de Almeida JPP, Turkarslan S, de Lomana ALG, et al. 2023. A genome-scale atlas reveals complex interplay of transcription and translation in an archaeon. mSystems 0:e00816–22. https://doi.org/10.1101/2022.08.31.505529
47. Grünberger F, Reichelt R, Bunk B, Spröer C, Overmann J, Rachel R, Grohmann D, Hausner W. 2019. Next generation DNA-seq and differential RNA-seq allow re-annotation of the *Pyrococcus furiosus* DSM 3638 genome and provide insights into archaeal antisense transcription. Front Microbiol 10:1603. https://doi.org/10.3389/fmicb.2019.01603
48. Chen S, Zhou Y, Chen Y, Gu J. 2018. Fastp: an ultra-fast all-in-one FASTQ preprocessor. Bioinformatics 34:i884–i890. https://doi.org/10.1093/bioinformatics/bty560
49. Langmead B, Salzberg SL. 2012. Fast gapped-read alignment with Bowtie 2. Nat Methods 9:357–359. https://doi.org/10.1038/nmeth.1923
50. Li H, Handsaker B, Wysoker A, Fennell T, Ruan J, Homer N, Marth G, Abecasis G, Durbin R, 1000 Genome Project Data Processing Subgroup. 2009. The sequence alignment/map format and SAMtools. Bioinformatics 25:2078–2079. https://doi.org/10.1093/bioinformatics/btp352
51. Love MI, Huber W, Anders S. 2014. Moderated estimation of fold change and dispersion for RNA-seq data with DESeq2. Genome Biol 15:550. https://doi.org/10.1186/s13059-014-0550-8
52. Liao Y, Smyth GK, Shi W. 2019. The R package *Rsubread* is easier, faster, cheaper and better for alignment and quantification of RNA sequencing reads. Nucleic Acids Res 47:e47. https://doi.org/10.1093/nar/gkz114
53. Bolger AM, Lohse M, Usadel B. 2014. Trimmomatic: a flexible trimmer for Illumina sequence data. Bioinformatics 30:2114–2120. https://doi.org/10.1093/bioinformatics/btu170
54. Smith T, Heger A, Sudbery I. 2017. UMI-tools: modeling sequencing errors in unique molecular identifiers to improve quantification accuracy. Genome Res 27:491–499. https://doi.org/10.1101/gr.209601.116
55. Grünberger F, Ferreira-Cerca S, Grohmann D. 2022. Nanopore sequencing of RNA and cDNA molecules in *Escherichia coli*. RNA 28:400–417. https://doi.org/10.1261/rna.078937.121
56. Adams PP, Baniulyte G, Esnault C, Chegireddy K, Singh N, Monge M, Dale RK, Storz G, Wade JT. 2021. Regulatory roles of *Escherichia coli* 5' UTR and ORF-internal RNAs detected by 3' end mapping. eLife 10:1–33. https://doi.org/10.7554/eLife.62438
57. Mo W, Liu B, Zhang H, Jin X, Lu D, Yu Y, Liu Y, Jia J, Long Y, Deng X, Cao X, Guo H, Zhai J. 2021. Landscape of transcription termination in Arabidopsis revealed by single-molecule nascent RNA sequencing. Genome Biol 22. https://doi.org/10.1186/s13059-021-02543-4
58. Grünberger F, Jüttner M, Knüppel R, Ferreira-Cerca S, Grohmann D. 2022. Insights into rRNA processing and modification mapping in archaea using nanopore-based RNA sequencing. Microbiology. https://doi.org/10.1101/2021.06.14.448286
59. Li H. 2021. New strategies to improve minimap2 alignment accuracy. Bioinformatics 37:4572–4574. https://doi.org/10.1093/bioinformatics/btab705
60. Li H. 2018. Minimap2: pairwise alignment for nucleotide sequences. Bioinformatics 34:3094–3100. https://doi.org/10.1093/bioinformatics/bty191
61. Wickham H, Averick M, Bryan J, Chang W, McGowan L, François R, Grolemund G, Hayes A, Henry L, Hester J, Kuhn M, Pedersen T, Miller E, Bache S, Müller K, Ooms J, Robinson D, Seidel D, Spinu V, Takahashi K, Vaughan D, Wilke C, Woo K, Yutani H. 2019. Welcome to the Tidyverse. JOSS 4:1686. https://doi.org/10.21105/joss.01686
62. Atanassov I, Urlaub H. 2013. Increased proteome coverage by combining PAGE and peptide isoelectric focusing: comparative study of GEL-based separation approaches. Proteomics 13:2947–2955. https://doi.org/10.1002/pmic.201300035
63. Meier F, Brunner AD, Koch S, Koch H, Lubeck M, Krause M, Goedecke N, Decker J, Kosinski T, Park MA, Bache N, Hoerning O, Cox J, Räther O, Mann M. 2018. Online parallel accumulation-serial fragmentation (PASEF) with a novel trapped ion mobility mass spectrometer. Mol Cell Proteomics 17:2534–2545. https://doi.org/10.1074/mcp.TIR118.000900
64. Meier F, Brunner AD, Frank M, Ha A, Bludau I, Voytik E, Kaspar-Schoenefeld S, Lubeck M, Raether O, Bache N, Aebersold R, Collins BC, Röst HL, Mann M. 2020. diaPASEF: parallel accumulation-serial fragmentation combined with data-independent acquisition. Nat Methods 17:1229–1236. https://doi.org/10.1038/s41592-020-00998-0
65. Schwanhäusser B, Busse D, Li N, Dittmar G, Schuchhardt J, Wolf J, Chen W, Selbach M. 2011. Global Quantification of mammalian gene expression control. Nature 473:337–342. https://doi.org/10.1038/nature10098
66. Ritchie ME, Phipson B, Wu D, Hu Y, Law CW, Shi W, Smyth GK. 2015. Limma powers differential expression analyses for RNA-sequencing and microarray studies. Nucleic Acids Res 43:e47. https://doi.org/10.1093/nar/gkv007
67. Baes R, Grünberger F, dit Ruys SP, Couturier M, De Keulenaer S, Skevin S, Van Nieuwerburgh F, Vertommen D, Grohmann D, Ferreira-Cerca S, Peeters E. 2022. Transcriptional and translational dynamics underlying heat shock response in the thermophilic Crenarchaeon *Sulfolobus acidocaldarius*. bioRxiv. https://doi.org/10.1101/2022.12.17.520879
68. Knüppel R, Trahan C, Kern M, Wagner A, Grünberger F, Hausner W, Quax TEF, Albers SV, Oeffinger M, Ferreira-Cerca S. 2021. Insights into synthesis and function of KsgA/Dim1-dependent rRNA modifications in archaea. Nucleic Acids Res 49:1662–1687. https://doi.org/10.1093/nar/gkaa1268
69. Makarova KS, Wolf YI, Koonin EV. 2015. Archaeal clusters of orthologous genes (arCOGs): an update and application for analysis of shared features between thermococcales, methanococcales, and methanobacteriales. Life (Basel) 5:818–840. https://doi.org/10.3390/life5010818
70. Young MD, Wakefield MJ, Smyth GK, Oshlack A. 2010. Gene ontology analysis for RNA-seq: accounting for selection bias. Genome Biol 11:R14. https://doi.org/10.1186/gb-2010-11-2-r14
71. Blombach F, Matelska D, Fouqueau T, Cackett G, Werner F. 2019. Key concepts and challenges in archaeal transcription. J Mol Biol 431:4184–4201. https://doi.org/10.1016/j.jmb.2019.06.020
72. Bailey TL, Boden M, Buske FA, Frith M, Grant CE, Clementi L, Ren J, Li WW, Noble WS. 2009. MEME SUITE: tools for motif discovery and searching. Nucleic Acids Res 37:W202–8. https://doi.org/10.1093/nar/gkp335
73. Wagih O. 2017. Ggseqlogo: a versatile R package for drawing sequence logos. Bioinformatics 33:3645–3647. https://doi.org/10.1093/bioinformatics/btx469

74. Blombach F, Fouqueau T, Matelska D, Smollett K, Werner F. 2021. Promoter-proximal elongation regulates transcription in archaea. Nat Commun 12:5524. https://doi.org/10.1038/s41467-021-25669-2
75. Dar D, Prasse D, Schmitz RA, Sorek R. 2016. Widespread formation of alternative 3' UTR isoforms via transcription termination in archaea. Nat Microbiol 1:16143. https://doi.org/10.1038/nmicrobiol.2016.143
76. Lorenz R, Bernhart SH, Höner Zu Siederdissen C, Tafer H, Flamm C, Stadler PF, Hofacker IL. 2011. Viennarna package 2.0. Algorithms Mol Biol 6:26. https://doi.org/10.1186/1748-7188-6-26
77. Mao X, Ma Q, Zhou C, Chen X, Zhang H, Yang J, Mao F, Lai W, Xu Y. 2014. DOOR 2.0: presenting operons and their functions through dynamic and integrated views. Nucleic Acids Res 42:D654–9. https://doi.org/10.1093/nar/gkt1048
78. Esteves AM, Graça G, Peyriga L, Torcato IM, Borges N, Portais JC, Santos H. 2019. Combined transcriptomics–metabolomics profiling of the heat shock response in the hyperthermophilic archaeon *Pyrococcus furiosus*. Extremophiles 23:101–118. https://doi.org/10.1007/s00792-018-1065-0
79. Szklarczyk D, Gable AL, Lyon D, Junge A, Wyder S, Huerta-Cepas J, Simonovic M, Doncheva NT, Morris JH, Bork P, Jensen LJ, Mering C von. 2019. STRING v11: protein–protein association networks with increased coverage, supporting functional discovery in genome-wide experimental datasets. Nucleic Acids Res 47:D607–D613. https://doi.org/10.1093/nar/gky1131
80. Sharp PM, Li WH. 1987. The codon adaptation index--a measure of directional synonymous codon usage bias, and its potential applications. Nucleic Acids Res 15:1281–1295. https://doi.org/10.1093/nar/15.3.1281
81. Santos H, da Costa MS. 2002. Compatible solutes of organisms that live in hot saline environments. Environ Microbiol 4:501–509. https://doi.org/10.1046/j.1462-2920.2002.00335.x
82. Yagi-Utsumi M, Sikdar A, Song C, Park J, Inoue R, Watanabe H, Burton-Smith RN, Kozai T, Suzuki T, Kodama A, Ishii K, Yagi H, Satoh T, Uchiyama S, Uchihashi T, Joo K, Lee J, Sugiyama M, Murata K, Kato K. 2020. Supramolecular tholos-like architecture constituted by archaeal proteins without functional annotation. Sci Rep 10:1540. https://doi.org/10.1038/s41598-020-58371-2
83. Weinberg MV, Schut GJ, Brehm S, Datta S, Adams MWW. 2005. Cold shock of a hyperthermophilic archaeon: *Pyrococcus furiosus* exhibits multiple responses to a suboptimal growth temperature with a key role for membrane-bound glycoproteins. J Bacteriol 187:336–348. https://doi.org/10.1128/JB.187.1.336-348.2005
84. Rodionova IA, Vetting MW, Li X, Almo SC, Osterman AL, Rodionov DA. 2017. A novel bifunctional transcriptional regulator of riboflavin metabolism in archaea. Nucleic Acids Res 45:3785–3799. https://doi.org/10.1093/nar/gkw1331
85. Yue L, Li J, Zhang B, Qi L, Li Z, Zhao F, Li L, Zheng X, Dong X. 2020. The conserved ribonuclease aCPSF1 triggers genome-wide transcription termination of archaea via a 3'-end cleavage mode. Nucleic Acids Res 48:9589–9605. https://doi.org/10.1093/nar/gkaa702
86. Novichkov PS, Kazakov AE, Ravcheev DA, Leyn SA, Kovaleva GY, Sutormin RA, Kazanov MD, Riehl W, Arkin AP, Dubchak I, Rodionov DA. 2013. Regprecise 3.0--a resource for genome-scale exploration of transcriptional regulation in bacteria. BMC Genomics 14:745. https://doi.org/10.1186/1471-2164-14-745
87. Lipscomb GL, Keese AM, Cowart DM, Schut GJ, Thomm M, Adams MWW, Scott RA. 2009. Surr: a transcriptional activator and repressor controlling hydrogen and elemental sulphur metabolism in *Pyrococcus furiosus*. Mol Microbiol 71:332–349. https://doi.org/10.1111/j.1365-2958.2008.06525.x
88. Reichelt R, Gindner A, Thomm M, Hausner W. 2016. Genome-wide binding analysis of the transcriptional regulator TrmBL1 in *Pyrococcus furiosus*. BMC Genomics 17:40. https://doi.org/10.1186/s12864-015-2360-0
89. Reichelt R, Ruperti KMA, Kreuzer M, Dexl S, Thomm M, Hausner W. 2018. The transcriptional regulator TFB-RF1 activates transcription of a putative ABC transporter in *Pyrococcus furiosus*. Front Microbiol 9:838. https://doi.org/10.3389/fmicb.2018.00838
90. Grünberger F, Reichelt R, Waege I, Ned V, Bronner K, Kaljanac M, Weber N, El Ahmad Z, Knauss L, Madej MG, Ziegler C, Grohmann D, Hausner W. 2020. CopR, a global regulator of transcription to maintain copper homeostasis in *Pyrococcus furiosus*. Front Microbiol 11:613532. https://doi.org/10.3389/fmicb.2020.613532
91. Makarova KS, Aravind L, Grishin NV, Rogozin IB, Koonin EV. 2002. A DNA repair system specific for thermophilic archaea and bacteria predicted by genomic context analysis. Nucleic Acids Res 30:482–496. https://doi.org/10.1093/nar/30.2.482
92. Majumdar S, Zhao P, Pfister NT, Compton M, Olson S, Glover CVC, Wells L, Graveley BR, Terns RM, Terns MP. 2015. Three CRISPR-Cas immune effector complexes coexist in *Pyrococcus furiosus*. RNA 21:1147–1158. https://doi.org/10.1261/rna.049130.114
93. López-García P, Forterre P. 1999. Control of DNA topology during thermal stress in hyperthermophilic archaea: DNA topoisomerase levels, activities and induced thermotolerance during heat and cold shock in *Sulfolobus*. Mol Microbiol 33:766–777. https://doi.org/10.1046/j.1365-2958.1999.01524.x
94. Boonyaratanakornkit BB, Simpson AJ, Whitehead TA, Fraser CM, El-Sayed NMA, Clark DS. 2005. Transcriptional profiling of the hyperthermophilic methanarchaeon *Methanococcus jannaschii* in response to lethal heat and non-lethal cold shock. Environ Microbiol 7:789–797. https://doi.org/10.1111/j.1462-2920.2005.00751.x
95. Kormas KA, Tivey MK, Von Damm K, Teske A. 2006. Bacterial and archaeal phylotypes associated with distinct mineralogical layers of a white smoker spire from a deep-sea hydrothermal vent site (9 degrees N, East Pacific rise). Environ Microbiol 8:909–920. https://doi.org/10.1111/j.1462-2920.2005.00978.x
96. Anantharaman V, Koonin EV, Aravind L. 2001. TRAM, a predicted RNA-binding domain, common to tRNA uracil methylation and adenine thiolation enzymes. FEMS Microbiol Lett 197:215–221. https://doi.org/10.1111/j.1574-6968.2001.tb10606.x
97. Taha, Siddiqui KS, Campanaro S, Najnin T, Deshpande N, Williams TJ, Aldrich-Wright J, Wilkins M, Curmi PMG, Cavicchioli R. 2016. Single TRAM domain RNA-binding proteins in archaea: functional insight from Ctr3 from the Antarctic methanogen *Methanococcoides burtonii*. Environ Microbiol 18:2810–2824. https://doi.org/10.1111/1462-2920.13229
98. Zhang B, Yue L, Zhou L, Qi L, Li J, Dong X. 2017. Conserved TRAM domain functions as an archaeal cold shock protein via RNA chaperone activity. Front Microbiol 8:1597. https://doi.org/10.3389/fmicb.2017.01597
99. Williams TJ, Lauro FM, Ertan H, Burg DW, Poljak A, Raftery MJ, Cavicchioli R. 2011. Defining the response of a microorganism to temperatures that span its complete growth temperature range (-2°C to 28°C) using multiplex quantitative proteomics. Environ Microbiol 13:2186–2203. https://doi.org/10.1111/j.1462-2920.2011.02467.x
100. Londei P. 2005. Evolution of translational initiation: new insights from the archaea. FEMS Microbiol Rev 29:185–200. https://doi.org/10.1016/j.femsre.2004.10.002
101. Benelli D, Londei P. 2011. Translation initiation in archaea: conserved and domain-specific features. Biochem Soc Trans 39:89–93. https://doi.org/10.1042/BST0390089
102. Gelsinger DR, Dallon E, Reddy R, Mohammad F, Buskirk AR, DiRuggiero J. 2020. Ribosome profiling in archaea reveals leaderless translation, novel translational initiation sites, and ribosome pausing at single codon resolution. Nucleic Acids Res 48:5201–5216. https://doi.org/10.1093/nar/gkaa304
103. Schmitt E, Coureux PD, Kazan R, Bourgeois G, Lazennec-Schurdevin C, Mechulam Y. 2020. Recent advances in archaeal translation initiation. Front Microbiol 11:584152. https://doi.org/10.3389/fmicb.2020.584152
104. Moll I, Grill S, Gründling A, Bläsi U. 2002. Effects of ribosomal proteins S1, S2 and the DeaD/CsdA DEAD-box helicase on translation of leaderless and canonical mRNAs in *Escherichia coli*. Mol Microbiol 44:1387–1396. https://doi.org/10.1046/j.1365-2958.2002.02971.x
105. Genuth NR, Barna M. 2018. The discovery of ribosome heterogeneity and its implications for gene regulation and organismal life. Mol Cell 71:364–374. https://doi.org/10.1016/j.molcel.2018.07.018
106. Grill S, Gualerzi CO, Londei P, Bläsi U. 2000. Selective stimulation of translation of leaderless mRNA by initiation factor 2: evolutionary implications for translation. EMBO J 19:4101–4110. https://doi.org/10.1093/emboj/19.15.4101
107. Liberek K, Lewandowska A, Zietkiewicz S. 2008. Chaperones in control of protein disaggregation. EMBO J 27:328–335. https://doi.org/10.1038/sj.emboj.7601970

108. Al Refaii A, Alix JH. 2009. Ribosome biogenesis is temperature-dependent and delayed in *Escherichia coli* lacking the chaperones DnaK or DnaJ. Mol Microbiol 71:748–762. https://doi.org/10.1111/j.1365-2958.2008.06561.x
109. René O, Alix JH. 2011. Late steps of ribosome assembly in *E. coli* are sensitive to a severe heat stress but are assisted by the HSP70 chaperone machine. Nucleic Acids Res 39:1855–1867. https://doi.org/10.1093/nar/gkq1049
110. Shore D, Albert B. 2022. Ribosome biogenesis and the cellular energy economy. Curr Biol 32:R611–R617. https://doi.org/10.1016/j.cub.2022.04.083
111. DiRuggiero J, Achenbach LA, Brown SH, Kelly RM, Robb FT. 1993. Regulation of ribosomal RNA transcription by growth rate of the hyperthermophilic archaeon, *Pyrococcus furiosus*. FEMS Microbiol Lett 111:159–164. https://doi.org/10.1111/j.1574-6968.1993.tb06379.x
112. Grünberger F, Jüttner M, Knüppel R, Ferreira-Cerca S, Grohmann D. 2023. Nanopore-based RNA sequencing deciphers the formation, processing, and modification steps of rRNA intermediates in archaea. RNA 29:1255–1273. https://doi.org/10.1261/rna.079636.123
113. Sas-Chen A, Thomas JM, Matzov D, Taoka M, Nance KD, Nir R, Bryson KM, Shachar R, Liman GLS, Burkhart BW, Gamage ST, Nobe Y, Briney CA, Levy MJ, Fuchs RT, Robb GB, Hartmann J, Sharma S, Lin Q, Florens L, Washburn MP, Isobe T, Santangelo TJ, Shalev-Benami M, Meier JL, Schwartz S. 2020. Dynamic RNA acetylation revealed by quantitative cross-evolutionary mapping. Nature 583:638–643. https://doi.org/10.1038/s41586-020-2418-2
114. Khoshnevis S, Dreggors-Walker RE, Marchand V, Motorin Y, Ghalei H. 2022. Ribosomal RNA 2'-*O*-methylations regulate translation by impacting ribosome dynamics. Proc Natl Acad Sci USA 119:e2117334119. https://doi.org/10.1073/pnas.2117334119
115. Jain S, Koziej L, Poulis P, Kaczmarczyk I, Gaik M, Rawski M, Ranjan N, Glatt S, Rodnina MV. 2023. Modulation of translational decoding by m6A modification of mRNA. Nat Commun 14:4784. https://doi.org/10.1038/s41467-023-40422-7
116. Vitreschak AG, Rodionov DA, Mironov AA, Gelfand MS. 2002. Regulation of riboflavin biosynthesis and transport genes in bacteria by transcriptional and translational attenuation. Nucleic Acids Res 30:3141–3151. https://doi.org/10.1093/nar/gkf433
117. Rodionov DA, Leyn SA, Li X, Rodionova IA. 2017. A novel transcriptional regulator related to thiamine phosphate synthase controls thiamine metabolism genes in archaea. J Bacteriol 199:e00743-16. https://doi.org/10.1128/JB.00743-16
118. Haase I, Mörtl S, Köhler P, Bacher A, Fischer M. 2003. Biosynthesis of riboflavin in archaea. Eur. J. Biochem 270:1025–1032. https://doi.org/10.1046/j.1432-1033.2003.03478.x
119. Lipscomb GL, Schut GJ, Scott RA, Adams MWW. 2017. Surr is a master regulator of the primary electron flow pathways in the order Thermococcales. Mol Microbiol 104:869–881. https://doi.org/10.1111/mmi.13668
120. Yang H, Lipscomb GL, Keese AM, Schut GJ, Thomm M, Adams MWW, Wang BC, Scott RA. 2010. Surr regulates hydrogen production in *Pyrococcus furiosus* by a sulfur-dependent redox switch. Mol Microbiol 77:1111–1122. https://doi.org/10.1111/j.1365-2958.2010.07275.x
121. Imdahl F, Vafadarnejad E, Homberger C, Saliba AE, Vogel J. 2020. Single-cell RNA-sequencing reports growth-condition-specific global transcriptomes of individual bacteria. Nat Microbiol 5:1202–1206. https://doi.org/10.1038/s41564-020-0774-1
122. Ma P, Amemiya HM, He LL, Gandhi SJ, Nicol R, Bhattacharyya RP, Smillie CS, Hung DT. 2023. Bacterial droplet-based single-cell RNA-seq reveals antibiotic-associated heterogeneous cellular states. Cell 186:877–891. https://doi.org/10.1016/j.cell.2023.01.002
123. Cummins C, Ahamed A, Aslam R, Burgin J, Devraj R, Edbali O, Gupta D, Harrison PW, Haseeb M, Holt S, Ibrahim T, Ivanov E, Jayathilaka S, Kadhirvelu V, Kay S, Kumar M, Lathi A, Leinonen R, Madeira F, Madhusoodanan N, Mansurova M, O'Cathail C, Pearce M, Pesant S, Rahman N, Rajan J, Rinck G, Selvakumar S, Sokolov A, Suman S, Thorne R, Totoo P, Vijayaraja S, Waheed Z, Zyoud A, Lopez R, Burdett T, Cochrane G. 2022. The European nucleotide archive in 2021. Nucleic Acids Res 50:D106–D110. https://doi.org/10.1093/nar/gkab1051
124. Perez-Riverol Y, Bai J, Bandla C, García-Seisdedos D, Hewapathirana S, Kamatchinathan S, Kundu DJ, Prakash A, Frericks-Zipper A, Eisenacher M, Walzer M, Wang S, Brazma A, Vizcaíno JA. 2022. The PRIDE database resources in 2022: a hub for mass spectrometry-based proteomics evidences. Nucleic Acids Res 50:D543–D552. https://doi.org/10.1093/nar/gkab1038